

# Optimization Applications as Quantum Performance Benchmarks

Thomas Lubinski,<sup>1,2</sup> Carleton Coffrin,<sup>3</sup> Catherine McGeoch,<sup>4</sup>  
 Pratik Sathe,<sup>5,6</sup> Joshua Apanavicius,<sup>7,8</sup> and David E. Bernal Neira<sup>6,9</sup>

(Quantum Economic Development Consortium (QED-C) collaboration)\*

<sup>1</sup>*Quantum Circuits Inc, 25 Science Park, New Haven, CT 06511*

<sup>2</sup>*QED-C Technical Advisory Committee on Standards and Performance Benchmarks*

<sup>3</sup>*Advanced Network Science Initiative, Los Alamos National Laboratory, USA*

<sup>4</sup>*D-Wave Systems, Burnaby, British Columbia, Canada, V5G 4M9, Canada*

<sup>5</sup>*Department of Physics and Astronomy, University of California at Los Angeles, USA*

<sup>6</sup>*Research Institute of Advanced Computer Science, Universities Space Research Association, Mountain View, CA, USA*

<sup>7</sup>*Indiana University Department of Physics, Bloomington, Indiana 47405, USA*

<sup>8</sup>*Indiana University Quantum Science and Engineering Center, Bloomington, Indiana 47405, USA*

<sup>9</sup>*Quantum Artificial Intelligence Laboratory, NASA Ames Research Center, Mountain View, CA, USA*

(Dated: February 7, 2023)

Combinatorial optimization is anticipated to be one of the primary use cases for quantum computation in the coming years. The Quantum Approximate Optimization Algorithm (QAOA) and Quantum Annealing (QA) have the potential to demonstrate significant run-time performance benefits over current state-of-the-art solutions. Using existing methods for characterizing classical optimization algorithms, we analyze solution quality obtained by solving Max-Cut problems using a quantum annealing device and gate-model quantum simulators and devices. This is used to guide the development of an advanced benchmarking framework for quantum computers designed to evaluate the trade-off between run-time execution performance and the solution quality for iterative hybrid quantum-classical applications. The framework generates performance profiles through effective visualizations that show performance progression as a function of time for various problem sizes and illustrates algorithm limitations uncovered by the benchmarking approach. The framework is an enhancement to the existing open-source QED-C Application-Oriented Benchmark suite and can connect to the open-source analysis libraries. The suite can be executed on various quantum simulators and quantum hardware systems.

## CONTENTS

I. Introduction	2	C. Result Quality and Time of Execution	9
II. Background	3	V. Execution on Quantum Hardware	12
A. Benchmarking Gate-Model Quantum Computers	3	A. Considerations	12
1. System-Level Benchmarks	3	B. Execution on Shared Quantum Hardware	12
2. Application-Level Benchmarks	4	C. Containerized Execution (Co-Location)	14
B. Benchmarking Quantum Annealing Computers	5	D. Effect of Circuit Parameterization	16
1. System-Level Benchmarks	5	E. Execution on Quantum Annealing Hardware	16
2. Application-Level Benchmarks	5	F. Discussion of Hardware Results	17
C. Quantum Benchmarks for Optimization Tasks	5	VI. Result Quality and Hyper-Parameters	18
1. Previous Work	5	A. Result Quality and Objective Functions	18
2. Our Approach	6	B. Initial Angles and Restarts	19
III. Quantum Heuristics for Optimization Problems	6	C. Fixed Angle Conjecture	20
A. Quantum Approximate Optimization Algorithm	6	D. Parameter Selection Strategy	21
B. Quantum Annealing	7	VII. Summary and Conclusions	23
IV. QED-C Benchmark Framework Enhancements	7	Code Availability	23
A. Benchmark Algorithms for QAOA and QA	8	Acknowledgement	24
B. Measuring Fidelity of QAOA Ansatz Execution	8	A. Methods for Combinatorial Optimization	25
		1. Combinatorial Optimization Theory	25
		B. Problem and Implementation Details	26
		References	27

\* This work was sponsored by the Quantum Economic Development Consortium (QED-C) and was performed under the auspices of the QED-C Technical Advisory Committee on Standards and Performance Benchmarks. The authors acknowledge many committee members for their input to and feedback on the project and this manuscript.

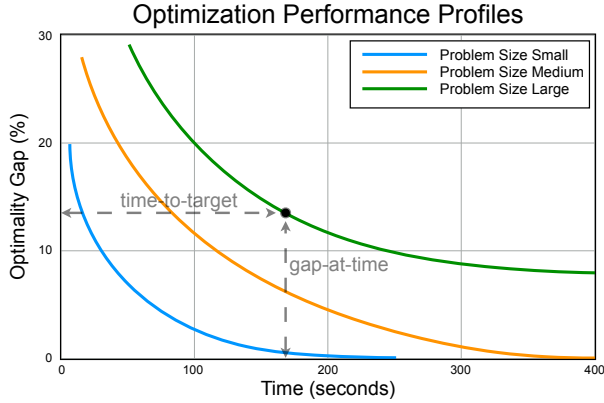


**FIG. 1: An Illustration of a Performance Profile for Benchmarking Optimization Methods.** Performance Profile plots, like the one shown here, are widely used by the Operations Research community to understand, communicate and compare the performance of optimization methods. Quality of solution, as the relative difference from optimal (optimality gap), can be seen to evolve over time during the execution of an optimization algorithm. This permits a user to gauge the time required to obtain a solution of a desired quality (time-to-target) or the solution quality that can be achieved after a specified amount of time (gap-at-time). The gap-at-time metric is the *de facto* standard used in Operations Research as it is reflective of use cases for the majority of industrial optimization applications. Performance profiles tend to change with problem size. It is common for problems with a small number of decision variables to converge to an optimal solution fairly quickly, while with larger problems it can be difficult to achieve solutions above a quality threshold, which is expected due to the NP-HARD nature of challenging optimization tasks.

## I. INTRODUCTION

In many application domains, it is of utmost importance to efficiently determine a near-optimal solution to problems that involve many variables which, in combination, affect the cost of some operation or function. For example, in a large power grid, rapidly determining the best allocation of power distribution could prevent a major blackout. These are known as combinatorial optimization problems, a class of which is often cited as a potential use case for quantum computing [1–3], as they typically involve a discrete search space that grows exponentially with respect to the size of the problem.

Classical computer algorithms for addressing such problems are substantially advanced and are implemented across industry, government, and academia as critical functions in optimizing the utilization of resources and minimizing cost. Combinatorial optimization applications are often executed under tight resource constraints (e.g., time, memory, energy, or money), and there is particular emphasis on quantifying the quality of results that could be obtained within a limited budget. Techniques for measuring and comparing the performance of alternative competing solutions have matured and are in broad use [1].

In the emerging world of quantum computing, new techniques for finding solutions to such combinatorial challenges, such as Quantum Annealing (QA) [4, 5] and the Quantum Ap-

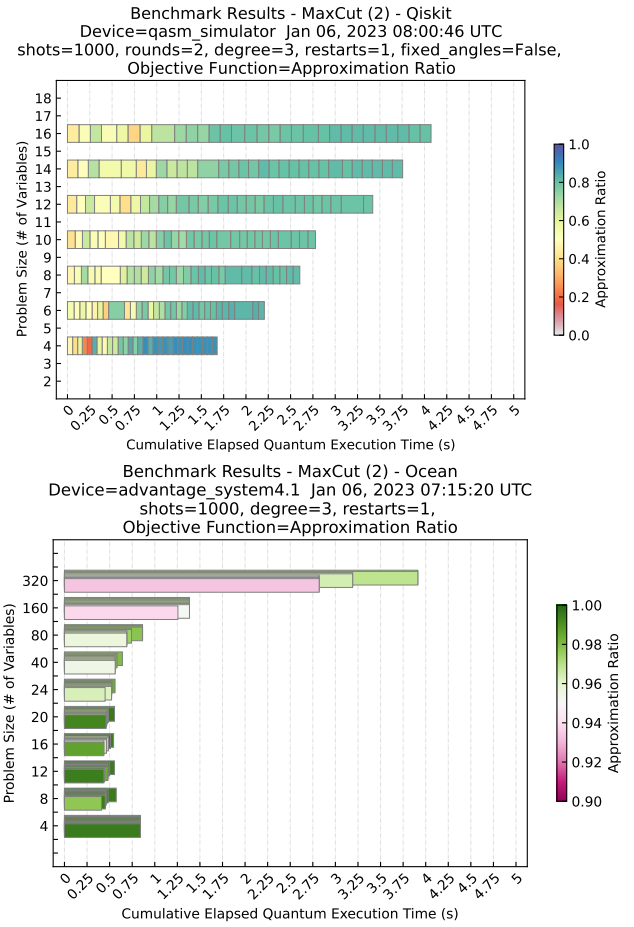


**FIG. 2: Characterizing Performance of Quantum Computing Solutions.** This new performance profile depicts the trade-off between result quality and execution time for two quantum computing solutions to the unweighted Max-Cut problem, the Quantum Approximate Optimization Algorithm (QAOA, top) and Quantum Annealing (QA, bottom). Each row shows a different problem size (= qubits), where the X-axis displays cumulative execution time, and the rectangle color is a measure of solution quality, the approximation ratio ( $= 1 - \text{opt\_gap}/100$ ). For QAOA, successive rectangles depict its iterative execution, tracking the search for appropriate parameters in an attempt at convergence to an optimal solution. For QA, each stacked rectangle represents a distinct execution at increasing anneal times. The benchmarking approach is explained in the text.

proximate Optimization Algorithm (QAOA) [6] may demonstrate some benefit over classical solutions applied to the same problem. Theory and classical simulations indicate that, for some problems, QAOA can outperform classical algorithms [7, 8] and a few empirical tests of QA systems have demonstrated superior performance over classical alternatives in limited scenarios [3, 9–11]. Numerous efforts have emerged to characterize or benchmark the performance of quantum computers and their applications in addressing optimization problems (see [section II](#)). However, we find that for such benchmarks to be accessible to users outside of academia and quantum computing developers, they must be integrated with emerging quantum computing benchmark suites and results

presented in a manner that is meaningful to experts within target domains, such as classical optimization and Operations Research (OR).

In this paper, we introduce a methodology for measuring the performance characteristics of quantum computing systems when executing combinatorial optimization applications that use the QA and QAOA algorithms and for evaluating the gate model and annealing styles of quantum computing side-by-side. We structure this to provide insight into unique aspects of quantum computing while maintaining a presentation recognizable to practitioners in the optimization field. Our methods exercise and stress multiple components of the integrated hybrid quantum-classical computer systems on which they run and mimic the load characteristics inherent in practical applications of this new technology. They uniformly capture, analyze, and present metrics associated with the execution of both models of quantum computing to support comparisons across architectures. As an illustration, we present several performance profiles obtained from this work in Figs. 1 and 2.

To demonstrate the benchmark framework, we selected the widely studied combinatorial optimization problem, Max-Cut [12], in which the goal is to find the maximum cut size of an undirected graph. It is representative of a class of optimization problems that are easy to specify but difficult to solve efficiently [13], NP-HARD problems. These often arise from mapping practical applications [14, 15] to computing hardware and can appear as subroutines in composite algorithms. The Max-Cut problem offers a simple early-stage target for evaluating the effectiveness of quantum computing solutions, yet allows us to develop a methodology that would work on practical, larger applications for which it will be necessary to incorporate constraints and other aspects that escalate the challenge.

Our benchmarking framework is provided as an enhancement to the existing open-source QED-C Application-Oriented Benchmark suite [16, 17]. This is a diverse collection of algorithmic benchmarks for evaluating the performance of quantum computers (on problems not currently related to optimization), with supporting functions for execution on multiple quantum computing systems and for collecting, analyzing, and presenting performance metrics in a uniform manner. Basing our work on this existing framework enabled our group to readily extend it with new functionality and to make our work easy to use and accessible to a broad audience of users.

Our contribution to benchmarking methodology may be seen as a successful demonstration of the adaptation of standard procedures for evaluating heuristic optimization solvers, deployed to run on distributed heterogeneous platforms, to the quantum scenario. We hope this work sheds light on the practical considerations associated with implementing combinatorial optimization solvers on quantum computing systems and provides an extensible mechanism to measure and record progress made in the evolution of quantum algorithms and computing systems.

The remainder of this paper is structured as follows. Background on the fundamentals related to benchmarking the performance of quantum computers and their applications is provided

in section II. We review the two leading heuristic quantum solutions for combinatorial optimization in section III. Enhancements made to the QED-C Application-Oriented Benchmarks suite are described in section IV where we describe the benchmark algorithms and examine results from execution on classically implemented quantum simulators, to a modest scale, and validate that results match expectations.

In section V, we present results obtained from the execution of these benchmarks on two gate model quantum hardware systems, highlighting execution time and several techniques for its reduction. We also demonstrate the benchmark framework on a quantum annealing processor, providing a practical means for users to quantify performance across quantum architectures. The discussion that follows in section VI highlights factors that impact result quality, trade-offs in parameter selection, and challenges to scalability inherent in quantum algorithms.

## II. BACKGROUND

Numerous methods exist to evaluate the performance of quantum computers. These range from device and component-level measures through system-level benchmarks to recent benchmarking models oriented towards the application itself, including those that address combinatorial optimization problems. In this section, we briefly review these in the context of their relevance to the new work we describe in this paper.

### A. Benchmarking Gate-Model Quantum Computers

There are multiple techniques for estimating the component-level performance of gate model quantum computing devices, e.g., randomized benchmarking [18, 19] and gate set tomography [20]. Hardware providers use these techniques to calibrate and test their systems, with particular emphasis on the impact of quantum noise, and often publish performance metrics extracted from the results of these experiments.

However, component-level metrics do not capture the net effect of many components functioning together or factors that emerge from the interconnection of these devices, such as crosstalk, or other dependencies. Consequently, it has become necessary to develop system-level benchmarks [21–24], all-encompassing metrics that characterize the overall performance characteristics of a quantum computer.

#### 1. System-Level Benchmarks

For gate model systems, Quantum Volume (QV) [22, 25] has gained significant traction, producing a single-number metric of a quantum computer’s general capability that captures the combined effects of qubit number and results fidelity. Exhaustive studies of QV suggest that no single number can summarize the many dimensions that make up a quantum computer’s performance characteristics however [26–29]. To address these limitations, Volumetric Benchmarking (VB) [23, 30] was proposed as a method by which the observed performance of the

quantum computing system is plotted in the two-dimensional depth  $\times$  width “volumetric” grid, illustrating its ability to execute both wide/shallow and deep/narrow circuits and extending the square circuits represented by QV [31].

QV and VB characterize quantum circuit execution quality and scale, but neither offers insight into the run time required for program execution, a key factor in evaluating solution viability. Recently, the Circuit Layer Operations per Second (CLOPS) was introduced [24] as a measure of run-time performance computed by executing a sequence of quantum volume circuits. CLOPS is designed to characterize speed, capturing the impact of circuit compilation, data transfer, execution and measurement run-time, and other latencies.

## 2. Application-Level Benchmarks

Extrapolating from component-level and system-level metrics to accurately predict application performance can be difficult and unreliable [23, 27]. New techniques have emerged to address this need for an approach to benchmarking gate model quantum computers in the context of the applications that will execute on them and to compare the performance of hardware platforms at an integrated system level.

Application-oriented benchmark frameworks typically use well-known quantum gate combinations or algorithms, provide inputs and expected outputs, and execute them on quantum simulators or physical hardware. Suites, such as QASMBench [32], SupermarQ [33], and QPack Scores [34] create and execute circuits programmatically, computing quality metrics of algorithms’ results, such as statistical differences between expected and actual measurements and nearness to an application-specific metric derived from the measurements.

Of particular relevance is the first QED-C application-oriented benchmark suite [16, 17], upon which our work is predicated. In this framework, performance is evaluated by executing a suite of algorithms, varying problem size programmatically, and mapping the quality of the results to circuit width and depth. This produces a fidelity gradient comprised of algorithm “profiles”, depicting the volumetric capacity of the quantum computer. An example of a volumetric plot composed of four algorithm profiles is shown in Figure 3. The QED-C benchmarks formed the basis for recent work by IonQ, in which a single-number metric called “Algorithmic Qubits” (AQ) [35] was proposed as a measure of performance derived from a quantum computer’s ability to execute these algorithms.

The QED-C benchmarks compute two figures of merit for the quality of the results obtained by executing a quantum circuit and comparing the final measurement distribution against what would be expected if executed on an ideal quantum computer. The simple Hellinger fidelity  $F_S$  is defined in Equation 1 where  $P_{\text{ideal}}$  and  $P_{\text{meas}}$  are the ideal and measured probability distributions [36]. To enable comparison of results across algorithms with different expected measurement densities, a normalized Hellinger fidelity  $F$  is defined in Equation 2 where

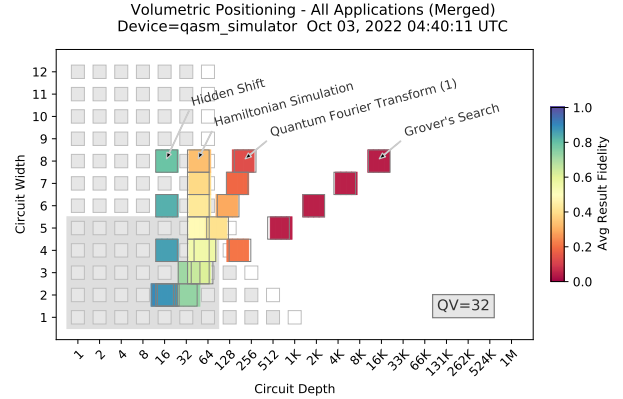


FIG. 3: **Application-Oriented Benchmarks.** Here, we present one way in which we present the result fidelity obtained by executing several application-oriented benchmarks up to 8 qubits on a noisy quantum computer simulator. The plot shows the average result fidelity as a function of circuit width and the circuit depth plotted on a volumetric background, in order to visualize the ‘profile’ and result fidelity of the benchmark circuits.

$P_{\text{uniform}}$  is a uniform random distribution [17].

$$F_S(P_{\text{ideal}}, P_{\text{meas}}) = \left( \sum_x \sqrt{P_{\text{meas}}(x)P_{\text{ideal}}(x)} \right)^2 \quad (1)$$

$$F(P_{\text{ideal}}, P_{\text{meas}}) = \frac{F_S(P_{\text{ideal}}, P_{\text{meas}}) - F_S(P_{\text{ideal}}, P_{\text{uniform}})}{1 - F_S(P_{\text{ideal}}, P_{\text{uniform}})} \quad (2)$$

Henceforth, we refer to the normalized Hellinger fidelity  $F$  as simply the circuit or result fidelity. A result fidelity of 0 corresponds to a uniformly random probability distribution, while a fidelity of 1 corresponds to the ideal probability distribution. (Note: the ‘raw’ normalized fidelity can be negative if the ideal distribution is closer to the uniform distribution than to the observed distribution, an effect that we remove by clamping to a value of 0.) Result fidelity is expected to decrease as the circuit width and depth increase, but many other factors can impact this metric [17].

Besides assessing a computer’s execution fidelity, the QED-C benchmarks capture detailed metrics related to execution time, subdividing the total time into components such as transpilation, load, initialization, and quantum execution times. The time required to execute circuits within a quantum application is an important metric of performance [37–40], often cited when comparing quantum and classical computations. E.g., the quantum and classical computing times were central to recent demonstrations of quantum advantage [41, 42].

This framework for capturing run-time metrics is foundational to our work in benchmarking hybrid algorithms for combinatorial optimization as presented in section IV. While execution time was included in the first QED-C benchmarks, it was intended that benchmarking of iterative hybrid algorithms would provide a more complete picture of a quantum computer’s run-time performance [17].

## B. Benchmarking Quantum Annealing Computers

Quantum computation based on quantum annealing techniques has been used to address combinatorial optimization problems for over a decade [3, 9, 11, 43, 44]. It is, therefore, essential that quantum annealing is included in both the analysis of benchmarking of quantum applications and in the enhanced suite of QED-C application-oriented benchmarks.

Large quantum annealing systems have been available for empirical study since the release of the 128-qubit D-Wave One in 2011 [45–47]. For this reason, quantum annealing benchmarking has tended to focus on application-oriented tests rather than system-level tests. A smaller body of work has developed hardware- and system-level benchmarks for characterizing the basic properties of quantum annealing hardware.

### 1. System-Level Benchmarks

Some examples of component- and system-level approaches to evaluating quantum annealing processors may be found in early papers demonstrating quantum properties by comparing small systems to theoretical models, such as [45, 48, 49]. More recently, protocols for validation and verification of large-scale quantum annealing hardware have been proposed [50–52] with a focus on characterizing the noise properties of such devices.

### 2. Application-Level Benchmarks

The vast majority of published benchmarking work in QA considers application-level tests [3, 53–55] using models with more than 100 qubits, which presents significant challenges for validation by comparison to the classical simulation of ideal (noise-free) quantum systems. Consequently, the bulk of this application benchmarking work compares the performance of quantum annealing hardware to classical methods, like Simulated Annealing [56], Parallel Tempering [57, 58] and Integer Programming [3, 59]. A key metric of interest in these works is runtime performance, where the runtime required of the quantum annealing hardware is compared to classical algorithms to achieve similar solution quality. These comparisons are often executed on synthetic optimization problems where a known optimal solution is planted as part of the instance generation algorithm [60–62].

## C. Quantum Benchmarks for Optimization Tasks

There is much background material available on benchmarking classical solutions to optimization problems [3, 59, 63] and comparing quantum methods to classical solutions [44, 64, 65]. Here, we focus on the challenges of benchmarking quantum solutions on real-world hardware, where the noise characteristics and runtime overheads of quantum computers introduce additional requirements for benchmarking.

## 1. Previous Work

Current research on classical solutions to optimization problems is often oriented toward improving the performance of quantum algorithms, separate from the analysis of specific hardware platforms. Such works seek to identify what types of optimization tasks might be possible with future (usually noise-free) quantum hardware [66]. Adapting this approach to QA and QAOA generally involves comparing different implementations or tuning strategies of the quantum algorithm, rather than performing runtime comparisons against classical algorithms. These studies are often limited to very small optimization tasks (e.g.,  $\leq 32$  qubits) so that classical emulation of an ideal quantum computer can be utilized. In these studies, the primary metrics of interest are expected solution quality and “operation counts” (i.e., circuit depth), which are used as an approximate measurement of run-time.

An important research question is to explore when quantum solutions to optimization problems may start outperforming state-of-the-art classical methods [3, 44, 59, 67, 68]. Such studies require 100’s of qubits to consider optimization tasks that are sufficiently time-consuming for current classical methods and hence could benefit quantum computing hardware.

Within this context, two main threads of execution time analysis have been used in comparing the performance of the quantum annealing algorithm to classical heuristics. The *time-to-solution* (TTS) metric determines the expected wall-clock time required to solve a problem to optimality [46, 67–70], while the *time-to-target* (TTT) metric determines the expected wall-clock time required to solve a problem to a specified *target* solution quality [3, 9, 44, 53]. The typical approach is to measure how TTS or TTT changes as a function of problem size for both the classical and quantum methods (i.e., a scaling advantage) so that one can forecast at what system sizes the quantum solution approach is likely to be faster than the classical one.

Due to the implementation complexity of configuring optimization tasks for benchmarking quantum hardware, a number of software frameworks have emerged to support the evaluation of the same (or similar) optimization methods implemented on different platforms. Benchmark frameworks such as SupermarQ [33] and QPack Scores [34] include one or more QAOA applications in their sample benchmarks, while QUARK [71] considers specific optimization problems arising in industry. The Q-score metric [72] is claimed to be applicable to quantum processors in several categories, measuring the size of the largest graph for which the solver outperforms random guessing within a fixed time limit. All references present results that measure solution validity, feasibility, and run-time on several backend quantum computers, some on both gate model and quantum annealing devices. Many of them are accompanied by a repository of open-source code that users are able to execute within their own environment.

## 2. Our Approach

Our effort has two primary goals: 1) to integrate and enhance key concepts from other optimization-centric benchmark efforts into the QED-C benchmark suite as a standard feature and 2) to present the results and analysis in ways that are recognizable by practitioners in the Operations Research (OR) field, already familiar with benchmarking classical solutions to optimization problems.

This section describes specific features of the framework we have developed for cross-paradigm benchmarking of quantum optimization heuristics. The enhancements made to our original benchmark framework are driven by specific features and challenges of optimization problems and of heuristic performance evaluation, which are distinct from the simple test scenarios used in our initial benchmark suite. The Operations Research (OR) community has developed methodologies and tools for evaluating computational performance in this context, some of which we have adapted to the quantum scenario. See Appendix A for a discussion of theoretical foundations.

Several features distinguish our benchmarking framework from others. Users are able to evaluate both execution time and solution quality in detail and explore the trade-offs (as opposed to fixing a specific TTS or TTT metric). The platform supports benchmarking of quantum computing hardware that can run quantum annealing or gate model algorithms. It also provides the ability to select problems and inputs of interest, beyond our simple illustrations using Max-Cut inputs. Presentation of benchmark results is aligned with standard methodologies of Operations Research and the QED-C framework. As quantum computers grow in size, the benchmark framework will be able to support testing on a wide variety of optimization problems.

## III. QUANTUM HEURISTICS FOR OPTIMIZATION PROBLEMS

The benchmarking framework measures performance characteristics of the two leading quantum heuristics for solving combinatorial optimization problems: the Quantum Approximate Optimization Algorithm (QAOA), which uses a gate-model quantum computer, and Quantum Annealing (QA), which uses an analog quantum computer. Throughout this paper, benchmarking of these algorithms is presented in the context of their application to solving the Max-Cut problem.

The input for a Max-Cut problem is an undirected graph consisting of nodes or vertices ( $V$ ) and edges ( $E$ ). (In general, each edge of the graph can be accompanied by a ‘weight’, but we only consider unweighted 3-regular graphs in this paper.) A cut is a partitioning of the nodes of the graph into two sets. The size of a cut is defined as the number of graph edges that connect nodes belonging to different sets. The Max-Cut problem is the task of identifying a cut that has the largest size out of all possible cuts.

Max-Cut has emerged as a popular benchmark for quantum optimization [12, 73] for two reasons: (1) it is among the most challenging combinatorial optimization tasks, even to obtain an approximate solution, i.e., APX-Hard [13, 74], (2)

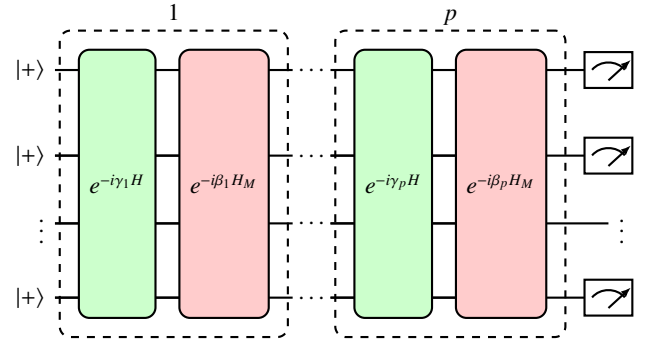


FIG. 4: **The QAOA circuit** consists of  $p$  repeating parameterized blocks. First, each qubit is acted upon with the Hadamard gate, to obtain the  $|+\rangle$  state. Each block further consists of a rotation involving the problem Hamiltonian  $H$ , followed by a rotation involving the mixer Hamiltonian  $H_M$ . Finally, all the qubits are measured in the computational basis  $\{|0\rangle, |1\rangle\}$ .

as an unconstrained discrete optimization task, it has a natural encoding as a Quadratic Unconstrained Binary Optimization (QUBO) [66, 75] or an Ising model [5, 76], ideally fitting current quantum optimization algorithms (QAOA, QA). While Max-Cut provides a reasonable first step for benchmarking current methods, testing more complex optimization tasks, including problems with constraints, will be important in future work to demonstrate that quantum-accelerated optimization can have an impact on a broad range of optimization applications.

### A. Quantum Approximate Optimization Algorithm

The Quantum Approximate Optimization Algorithm [77] is arguably the leading candidate for solving combinatorial optimization problems using gate-model quantum processors. QAOA belongs to the class of Variational Quantum Algorithms (VQA) [78] and is usually implemented iteratively wherein a classical optimizer ‘trains’ a parameterized quantum circuit. QAOA is a heuristic that attempts to solve combinatorial optimization problems such as QUBO problems. Specifically, the problem is encoded in the form of a specified quadratic function of binary variables, and the objective is to find an assignment for those variables that minimize the function.

At the core of QAOA is an ‘ansatz circuit’, which is a parameterized quantum circuit. Measurements in the computational basis at the end of the circuit correspond to sampling from a probability distribution over possible answers to the problem. A classical optimizer is employed to obtain parameter values that have a significant probability for optimal, or near-optimal solutions. Finally, repeatedly measuring the circuit with the parameter values determined by the optimizer provides approximate solutions to the problem.

The problem is first codified in the form of a Hamiltonian  $H_P$ , such that an optimal problem solution corresponds to a ground state(s), or lowest energy eigenstate(s). For a given choice of the number of ‘rounds’ denoted by  $p$ , the QAOA

ansatz is given by

$$|\beta, \gamma\rangle = e^{-i\beta_p H_M} e^{-i\gamma_p H_P} \dots e^{-i\beta_1 H_M} e^{-i\gamma_1 H_P} |+\rangle, \quad (3)$$

where  $H_M = \sum_i X_i$ , is the so-called mixer Hamiltonian, and  $|+\rangle = \otimes_i H |0\rangle$  is the equal superposition state. Here,  $X$  is the Pauli X matrix, defined via  $X|0\rangle = |1\rangle$  and  $X|1\rangle = |0\rangle$ . The ansatz state is thus obtained by implementing repeating and alternating rotations about  $H_P$  and  $H_M$  as shown in [Figure 4](#).

The Max-Cut problem can be framed in terms of obtaining the ground state of the Hamiltonian

$$H_P = \frac{-1}{2} \sum_{\langle i, j \rangle \in E} (1 - Z_i Z_j), \quad (4)$$

where  $E$  denotes the set of (undirected) edges of the graph, and  $Z$  is the Pauli-Z matrix satisfying  $Z|0\rangle = |0\rangle$  and  $Z|1\rangle = -|1\rangle$ . Each computational basis vector corresponds to a possible cut, and its energy represents the negative of the cut size. Note that the eigenvalues of  $H_P$  are all non-negative integers.

In order to characterize the quality of solutions, a quantity called the approximation ratio is usually computed. The approximation ratio  $r$  is defined as the ratio of the energy expectation value  $F_{\beta, \gamma} := \langle \beta, \gamma | H_P | \beta, \gamma \rangle$ , and the ground state energy value  $E_{\min}$ :

$$r_{\beta, \gamma} = \frac{F_{\beta, \gamma}}{E_{\min}} = \frac{\langle \beta, \gamma | H_P | \beta, \gamma \rangle}{E_{\min}}. \quad (5)$$

Note that the numerator is less than or equal to zero, while the denominator, which is the negative of the largest cut size, is strictly negative. Consequently,  $0 \leq r \leq 1$ . The classical optimizer routine aims to obtain optimal values of the angles  $\beta$  and  $\gamma$ , i.e., values that correspond to the highest value of the approximation ratio.  $F_{\beta, \gamma}$ , and hence  $r_{\beta, \gamma}$  cannot be computed exactly, and are instead approximated by measuring  $|\beta, \gamma\rangle$  many (say  $M$ ) times, or *shots*, in the computational basis at the end of the circuit (see [Figure 4](#)). Specifically,  $F_{\beta, \gamma}$  are approximated by the empirical average of energy.

## B. Quantum Annealing

With quantum annealing, an optimization problem is encoded into the machine, after which the solution is determined through quantum adiabatic evolution to arrive at a near-optimal final state. The algorithmic approach of quantum annealing is to leverage the dynamic evolution of a quantum system to transform an *initial* ground state (which is easy to prepare) into the ground state of a *target* Hamiltonian, which is unknown and difficult to compute by other means. At a high level, the protocol strives to identify the low-energy states of a user-specified  $H_{\text{Target}}$  model by conducting an analog interpolation process of the following Hamiltonian:

$$H(s) = (1 - s)H_{\text{Init}} + (s)H_{\text{Target}}. \quad (6)$$

The interpolation process starts with  $s = 0$  and in the ground state of  $H_{\text{Init}}$ . The annealing process consists of a smooth interpolation of  $s$  from 0 to 1. For a sufficiently long annealing

time, the adiabatic theorem demonstrates that a quantum system remains at the minimal eigenvector of the interpolating Hamiltonian,  $H(s)$  [79–81], and therefore arrives at minimum energy states of  $H_{\text{Target}}$  at the end of the evolution.

Currently available quantum annealing hardware focuses on a special case of [Equation 6](#) that is limited to the Transverse Field Ising model,

$$H(s) = A(s) \left( \sum_i X_i \right) + B(s) \left( \sum_i h_i Z_i + \sum_{i, j} J_{ij} Z_i Z_j \right). \quad (7)$$

Where  $X_i$  denotes the Pauli X operator applied to qubit  $i$ ,  $Z_i$  denotes the Pauli Z operator applied to qubit  $i$ , and  $Z_i Z_j$  is the tensor product of Z operators on qubits  $i$  and  $j$ . The two interpolation functions  $A(s)$  and  $B(s)$  control a transition from a strong  $H_{\text{Init}}$  and weak  $H_{\text{target}}$  to a weak  $H_{\text{Init}}$  and strong  $H_{\text{target}}$ ; that is,  $A(0) \gg B(0)$  and  $A(1) \ll B(1)$ . Through these functions, the hardware implements a default annealing “path”, which can be modified somewhat by user parameters. In this way, this hardware and the QA algorithm can find ground and low-energy states of a user-specified classical Ising model that is specified on the Z basis via the parameters  $h$  and  $J$ , which encode the local fields and coupling strengths, respectively. Note that the Max-Cut problem considered by this work is encoded in this model by setting  $h = 0$  and  $J_{ij} = -1$  for each edge  $i, j \in E$  that appears in the given Max-Cut graph. If the Max-Cut graph cannot be encoded naively in the quantum annealing hardware (i.e., the edge set of the Max-Cut problem is not a subgraph of the  $Z_i Z_j$  terms in the quantum annealing hardware), then a process known as *minor embedding* [82] is used to map the Max-Cut problem into a mathematically equivalent hardware-native problem.

It is interesting to notice that the QAOA algorithm outlined in [section III A](#), can be interpreted as a Trotterized version of [Equation 7](#) where the Trotter order is determined by the number of rounds  $p$ . That is, the smooth analog QA transition can be modeled by the limit of a QAOA circuit as  $p \rightarrow \infty$ . The computation of the approximation ratio is accomplished for QA in the same way as QAOA, by transforming the samples obtained after annealing to an equivalent distribution.

## IV. QED-C BENCHMARK FRAMEWORK ENHANCEMENTS

The QED-C Application-Oriented Benchmark suite reviewed in [section II A 2](#) is designed to control the execution of a quantum application over a range of problem sizes, capture metrics associated with its execution, and present those metrics in relevant ways [17]. Here, we build upon this framework, enhancing it with application-specific quality and temporal metrics associated with iterative hybrid quantum applications, where the trade-off between resource usage, here execution time, and solution quality is of importance. The approach is made functional for both gate model and quantum annealing computers.

To demonstrate the key enhancements, we focus on its application to a combinatorial optimization problem, using Max-Cut

**Algorithm1** Benchmark Algorithm for QAOA

```

1: target  $\leftarrow$  backend_id
2: initialize_metrics()
3: for size  $\leftarrow$  min_size, max_size do
4:   circuit_def  $\leftarrow$  define_problem(problem, size, args, rounds)
5:   for restart_id  $\leftarrow$  1, max_restarts do
6:     cost_function  $\leftarrow$  define_cost_function(problem)
7:     circuit, num_params  $\leftarrow$  create_circuit(circuit_def)
8:     cached_circuit  $\leftarrow$  compile_circuit(circuit)
9:     params[ $\beta, \gamma$ ]  $\leftarrow$  random(num_params)
10:    while minimizer() not done do  $\triangleright$  minimizing
11:      circuit  $\leftarrow$  apply_params(cached_circuit, params)
12:      counts  $\leftarrow$  execute(target, circuit, num_shots)
13:      energy, quality  $\leftarrow$  cost_function(counts)
14:      store_iteration_metrics(quality, timing)
15:      params[ $\beta, \gamma$ ]  $\leftarrow$  optimize(params[ $\beta, \gamma$ , energy])
16:      done  $\leftarrow$  True if lowest(energy) found
17:    end while
18:    compute_and_store_restart_metrics()
19:  end for
20:  compute_and_store_group_metrics()
21: end for

```

as a specific example. Different from the simple algorithms used in the initial benchmark suite, where circuit execution fidelity is the key metric (as described in [section II C](#)), the enhanced benchmark must derive a solution quality metric that is application-specific and accounts for the fact that solutions to optimization problems are often approximate. Results from its execution on a classically-implemented circuit-based quantum simulator illustrate how key metrics are collected and presented.

**A. Benchmark Algorithms for QAOA and QA**

Quantum annealing and circuit-based quantum computers solve a combinatorial optimization problem using fundamentally different strategies (QA vs QAOA, [section III](#)). Here, we detail the related algorithms used for benchmarking these solutions and highlight differences between them and how these impact the results, omitting some details for brevity.

Both algorithms operate on a target system *backend\_id* to solve a *problem* with input *args* and share an outer loop over a range of problem sizes [*min\_size, max\_size*], which encloses a second loop over a selectable number of restarts [1, *max\_restarts*]. The primary difference lies within the restart loop, where the QAOA and QA solvers are applied to the input, and the solution quality is evaluated over increasing execution times.

*a. Benchmarking QAOA* The QAOA benchmarking method is defined in [Algorithm 1](#). Nested within the first and second for loops is the QAOA algorithm, which defines a *cost\_function* based on the problem specifics and a gate model quantum circuit a number of *rounds* (often referred to as *p* in code) implementing the Hamiltonian associated with the problem. Starting with a random or fixed set of circuit parameters *params*, a classical optimizer applies these and executes the circuit to obtain measurement *counts* and compute a cost function. Classical optimizer code explores the parameter landscape by varying the set of parameters to obtain measurement counts that represent the lowest energy state for the Hamiltonian. A relevant *quality* metric is calculated and stored along with metrics that track the quantum and classical *timing* information. While we use random starting parameters for the benchmark, in practice users may have some information about a reasonable starting point, which could result in a better or quicker solution (see [section VI C](#)).

**Algorithm2** Benchmark Algorithm for QA

```

1: target  $\leftarrow$  backend_id
2: initialize_metrics()
3: for size  $\leftarrow$  min_size, max_size do
4:   for restart_id  $\leftarrow$  1, max_restarts do
5:     compute_quality  $\leftarrow$  define_compute_quality(problem)
6:     for a_time  $\leftarrow$  min_anneal_time, max_anneal_time do
7:       embedding  $\leftarrow$  define_problem(problem, size, args)
8:       sampler  $\leftarrow$  create_sampler(target, embedding)
9:       samples  $\leftarrow$  sample_ising(sampler, a_time, reads)
10:      quality  $\leftarrow$  compute_quality(samples)
11:      store_iteration_metrics(quality, timing)
12:    end for
13:    compute_and_store_restart_metrics()
14:  end for
15:  compute_and_store_group_metrics()
16: end for

```

ters *params*, a classical optimizer applies these and executes the circuit to obtain measurement *counts* and compute a cost function. Classical optimizer code explores the parameter landscape by varying the set of parameters to obtain measurement counts that represent the lowest energy state for the Hamiltonian. A relevant *quality* metric is calculated and stored along with metrics that track the quantum and classical *timing* information. While we use random starting parameters for the benchmark, in practice users may have some information about a reasonable starting point, which could result in a better or quicker solution (see [section VI C](#)).

*b. Benchmarking QA* The QA benchmarking method is described in [Algorithm 2](#). With quantum annealing, convergence to a solution is performed entirely within the quantum system, out of view of the user. The problem is embedded into a quantum state initialized on the hardware and the system is set to anneal towards a solution. The longer the system is permitted to anneal, the higher the solution quality that will be read. To provide a comparable measure of the time vs quality trade-off, benchmarking QA involves repeatedly executing the annealing process but varying the *anneal\_time* and querying (*reads*) *samples* the same number times as we do shots in QAOA. As with benchmarking QAOA, a relevant *quality* metric is calculated and stored along with metrics that track the quantum and classical *timing* information.

**B. Measuring Fidelity of QAOA Ansatz Execution**

Each iteration of the QAOA algorithm involves repeatedly measuring a parameterized circuit (corresponding to  $|\beta, \gamma\rangle$  from [Equation 3](#) and lines 12-15 of [algorithm 1](#)), with the parameter values determined by a classical optimizer routine (or set by the user in the first iteration). The success of the algorithm relies on the ability of the quantum subroutine to compute an accurate value of the objective function. If the measurement probabilities obtained by the quantum subroutine do not match sufficiently well with the probabilities from the ideal distribution  $P_{\text{ideal}}(s) = |\langle s | \beta, \gamma \rangle|^2$ , the effectiveness of

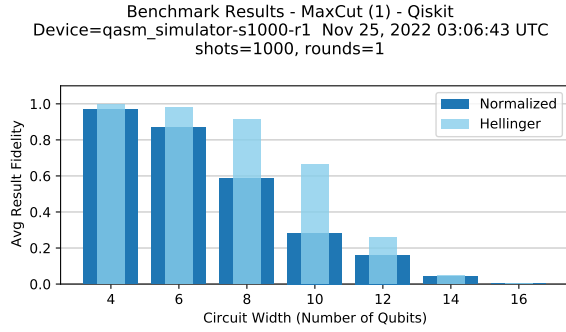


FIG. 5: **Fidelity of Ansatz Execution and Impact of Shots.** Here, we illustrate the difference in fidelity when executing the Max-Cut ansatz circuit at circuit widths ranging from 4 to 16 qubits, with 1000 shots and again with 5000 shots, on an ideal quantum simulator (using the same initial rounds and parameters). For each problem size, we use a single graph, which defines an *instance* of the Max-Cut problem. The resulting fidelity is greater when using a larger number of shots. The normalized and Hellinger fidelity computation is explained in the text.

the classical optimizer can be negatively impacted.

Multiple factors can affect fidelity. Even on a noiseless simulator, perfect fidelity can be achieved only within the limit of an infinite number of shots. On quantum hardware, noise and decoherence can exacerbate the drop in fidelity, as can limited connectivity between qubits. (See [section V](#) for more information about execution on physical devices.) To quantify circuit fidelity, we show both the Hellinger fidelity and the normalized Hellinger fidelity as defined in [section II A 2](#) and originally in [\[17\]](#). The normalized fidelity is most useful in our context, recalling that a circuit fidelity of 0 corresponds to a uniformly random probability distribution, while a fidelity of 1 corresponds to the ideal probability distribution.

On a noiseless simulator, the number of measurements per iteration (which we call the number of ‘shots’) has a significant effect on the circuit fidelity. For example, [Figure 5](#) shows that the circuit fidelity on a noiseless simulator is observed to be below 0.6 at 8 qubits when the number of shots is set to 1000, while it does so at 12 qubits when the number of shots is set to 5000. As the width of the circuit becomes larger, the number of shots required to distinguish between the ideal and random distributions increases, and it becomes more difficult to compute an accurate measure of result fidelity, as seen in the difference between the Hellinger and normalized fidelities.

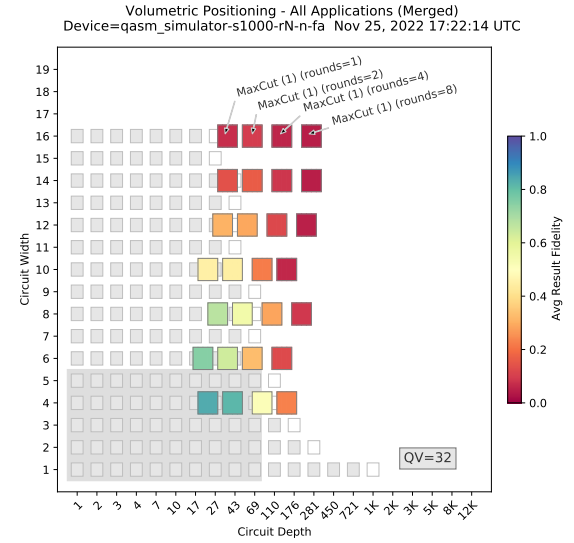


FIG. 6: **Volumetric Presentation of Fidelity and Impact of Rounds.** The fidelity metrics obtained for the execution of any quantum circuit are influenced by both the width of the circuit as well as its depth, or its total number of quantum gate layers. Here, the Max-Cut ansatz circuit with a varying number of rounds is executed on a noisy quantum simulator with a quantum volume of 32 (one- and two-qubit gate error rates 0.003 and 0.03, respectively). The (normalized) result fidelity at a specific width and depth is represented by the color shown in the rectangle at that location and degrades with increasing rounds (depth) or problem size (width).

Execution fidelity is expected to degrade not only as circuits become wider (i.e., comprise more qubits), but also deeper (i.e., have a larger number of gate layers). The volumetric plot in [Figure 6](#) uses a color scale to represent fidelity at specific widths and depths. It illustrates how circuit fidelity is impacted as one of the arguments to the QAOA ansatz definition, the number of [rounds](#) (referred to as  $p$  in code), is increased from 1 to 8. In this case, the circuit was executed with 1000 shots on a quantum simulator with noise characteristics that mimic a typical quantum computer (one- and two-qubit gate error rates 0.003 and 0.03, respectively) and with a quantum volume equal to 32 (the region shown in the dark rectangle). As the ‘rounds’ parameter becomes larger, the circuit becomes correspondingly deeper, and the result fidelity degrades as a function of depth.

### C. Result Quality and Time of Execution

The QAOA algorithm executes its ansatz circuit multiple times in a hybrid quantum-classical loop to converge on a result. The QA algorithm similarly converges to a solution but does so by embedding a problem into a quantum state and annealing for a specified amount of time. In both cases, the quality of the results obtained is impacted by the length of time the algorithm is permitted to execute. Here, we show how benchmarking results are presented in comparable ways and describe the methods used to collect and analyze the metrics.

In [Figure 7](#), we illustrate the time versus quality trade-off

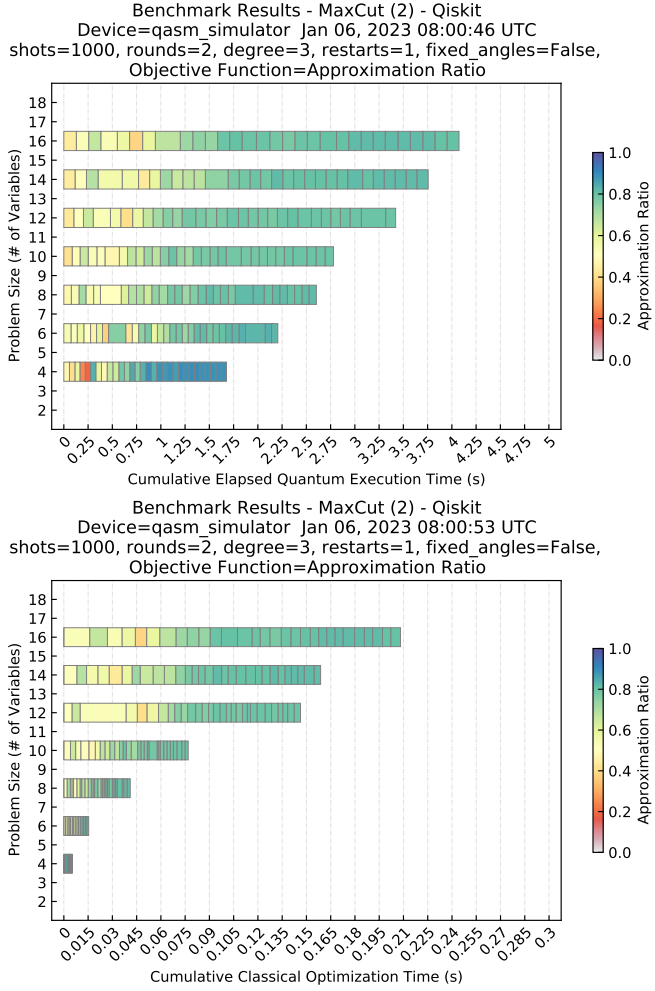


**FIG. 7: Iterative Execution of QAOA Max-Cut Algorithm.** In QAOA, a classical minimizer function iteratively executes an ansatz, varies its parameter values, and computes a cost function to converge to an optimal solution. The approximation ratio represents how closely the solution found matches a solution known to be correct (note: random sampling will produce a ratio of 0.5). In the first plot, each horizontal row represents successive iterations at each problem size (= number of qubits), where the position on the X-axis represents the cumulative quantum execution time, and color tracks the approximation ratio of the current classical optimizer iteration. In the second plot, the X-axis represents the cumulative classical computation time. For problems of this small size, the classical computation time is insignificant and can be largely ignored.

for the QAOA Max-Cut algorithm using a novel performance profile referred to as an ‘area plot’. Similar to the volumetric plot, it shows circuit width (problem size) on the Y-axis and uses the color of rectangles to illustrate a metric score. In this case, the horizontal width of an individual rectangle represents the execution time for a single ansatz, and its location along the X-axis indicates the cumulative execution time, including prior iterations. The metric score is an application-specific metric, such as the ‘approximation ratio’, derived by the algorithm from measurement results and parameters of the problem.

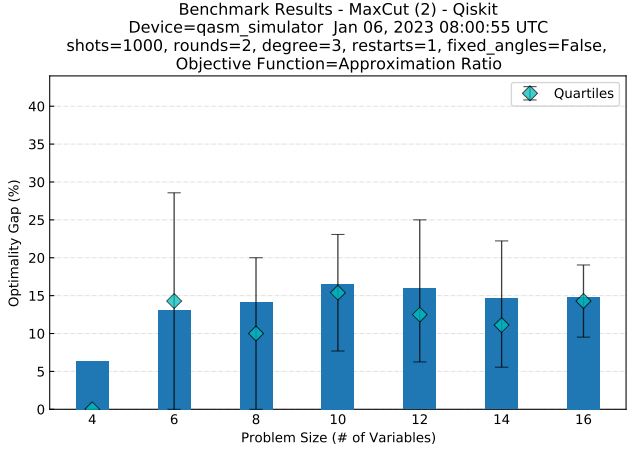


**FIG. 8: Showing Final Optimality Gap.** As the QAOA program executes, the minimizer finds an optimal solution to the Max-Cut problem, represented by the approximation ratio computed after the final iteration, seen in the rightmost rectangles of Figure 7. The optimality gap for each problem size is computed from those values and shown in this bar chart, along with quartile marks showing the distribution of the final measurement results. In some cases, result quality could improve with additional execution time, but we limit the benchmark to 30 iterations to conserve compute resources.

*a. Computing the Quality Score Metric* The QAOA and QA algorithms attempt to converge on a solution to an optimization problem by finding the lowest energy state of a Hamiltonian after a sequence of parameter tests (QAOA) or annealing operations (QA) on a target system. QAOA computes an energy value from measurement results and uses a classical optimizer to search for parameters that yield the lowest energy. QA does this by mapping the problem into an Ising model and annealing for a period of time, after which energy samples are taken. In both cases, the result is an energy value that can be compared against the actual optimal solution (i.e., the lowest energy of the Hamiltonian). The ratio between actual and expected, the “approximation ratio” defined in section II A, is used as the scoring metric shown in Figure 7. From this plot, a user can readily see the improvement in quality that occurs as execution progresses. The vertical grid visually gauges the quality of the results that can be expected after a specific time of execution. Shown here for QAOA, this presentation methodology applies to QA as well and can be seen in section V where hardware results are presented.

Note that the QAOA ansatz circuit starts in a uniform superposition. When executed under control of the optimizer, sampling a completely random distribution will yield an approximation ratio greater than 0.5 (see Figure 22). The optimizer may or may not converge to a better ratio, depending on the level of noise in the quantum system [66, 83–86].

In benchmarking of classical algorithms for optimization problems, it is common to report the quality of the result in terms of its distance from an optimal solution. This distance is referred to as the ‘optimality gap’ and is defined for our context in Equation 8. For each problem size, the quality of the result in the last iteration of Figure 7 is presented in Figure 8

as a bar chart showing the optimality gap along with a quartile representation of the distribution of results at all gaps.

$$\text{optimality\_gap} = (1.0 - \text{approximation\_ratio}) \times 100 \quad (8)$$

**b. Execution Time in QAOA** The total amount of time consumed by the QAOA algorithm includes both quantum and classical components. There is time related to the execution of the quantum ansatz circuit on the quantum processor. Additionally, there is time spent on a classical processor to perform the minimization function that computes new parameters from measurements obtained after each execution of the ansatz.

The time to execute the quantum portion of the algorithm itself is broken down into several components. One of these is the ‘Quantum Execution Time’, defined as the time to execute  $N$  shots of a quantum circuit within a quantum processor. This time is typically reported by quantum computer hardware providers in a result record and includes the time required to initialize the quantum system prior to execution, and the delay between shots [24]. as shown in [Equation 9](#).

$$t_{\text{quantum}} = t_{\text{init}} + N_{\text{shots}} \cdot (t_{\text{shot}} + t_{\text{delay}}) \quad (9)$$

Using QAOA, a quantum circuit is executed repeatedly but with varying parameters. The total time to execute the circuit, the ‘Elapsed Quantum Execution Time’, includes the time required to either compile the circuit or to apply parameters prior to execution, and to validate and load the compiled circuit for execution. Another highly variable component of the total is the time spent in a queue awaiting execution. Elapsed quantum execution time is defined in [Equation 10](#) and must be collected as part of the benchmarking algorithm as we did not find this metric to be directly available on most systems.

$$t_{\text{elapsed\_quantum}} = t_{\text{queue}} + t_{\text{compile}} + t_{\text{load}} + t_{\text{quantum}} \quad (10)$$

The sum of the quantum and elapsed quantum times for all iterations of the QAOA algorithm, the ‘Cumulative Quantum Execution Time’ and ‘Cumulative Elapsed Quantum Execution Time’ respectively, are defined in [Equation 11](#) and [12](#). The financial cost of quantum computation is often tied to the cumulative quantum execution time on many hardware systems. The elapsed time for each iteration is dependent on the parameters of execution and may be influenced by the system’s ability to support parameterized execution or the inclusion of hidden classical post-processing time, such as error mitigation. In [section V D](#), these are illustrated in the context of execution on quantum hardware.

$$t_{\text{cum\_quantum}} = \sum_{\text{iter}=1}^{N_{\text{iter}}} t_{\text{quantum}(\text{iter})} \quad (11)$$

$$t_{\text{cum\_elapsed\_quantum}} = \sum_{\text{iter}=1}^{N_{\text{iter}}} t_{\text{elapsed\_quantum}(\text{iter})} \quad (12)$$

‘Classical Execution Time’ for QAOA is the sum of the time needed to create the ansatz with specific parameters and time

used by the minimizer to process measurement results and generate new parameters during a specific iteration  $\text{iter}$ , as in [Equation 13](#). The ‘Cumulative Classical Execution Time’ is the sum of the classical execution times for all iterations as in [Equation 14](#). For small problems, this time is typically insignificant but can grow rapidly with problem size and rounds. It may also be impacted by the system’s ability to support parameterized execution and reduce creation time ([section V D](#)).

$$t_{\text{classical}} = t_{\text{create}} + t_{\text{optimize}} \quad (13)$$

$$t_{\text{cum\_classical}} = \sum_{\text{iter}=1}^{N_{\text{iter}}} t_{\text{classical}(\text{iter})} \quad (14)$$

The total time of execution for QAOA is the sum of the cumulative elapsed quantum time  $t_{\text{cum\_elapsed\_quantum}}$ , and classical compute time  $t_{\text{cum\_classical}}$ . Variability due to different processing options or choice of classical optimizer can result in widely differing result quality and execution times.

**c. Execution time in QA** For QA, the ‘Quantum Execution Time’ is defined as the time taken to execute  $N$  reads (samples) using a specified anneal time. This time is reported by the hardware as ‘qpu\_access\_time’ and includes ‘qpu\_programming\_time’ of  $\sim 16ms$  and the ‘anneal\_time’ multiplied by the number of reads along with other factors that contribute to total Quantum Processing Unit (QPU) sampling time (e.g., readout time of  $\sim 0.25ms$ ). Quantum execution time is defined in [Equation 15](#).

$$t_{\text{quantum}} = t_{\text{qpu\_access}} = t_{\text{qpu\_programming}} + t_{\text{qpu\_sampling}} \quad (15)$$

The ‘Elapsed Quantum Execution Time’ includes the time required to issue the sample command to the (remote) backend hardware system, wait for it to complete, and to receive a fully resolved sample set. It is defined in [Equation 16](#) and includes the quantum execution time, along with the time for computing a minor embedding of the input to match the specific qubit connection structure inside the QPU. This cost is measured once for each annealing time that we test (not always necessary in practice because embeddings can be reused).

$$t_{\text{elapsed\_quantum}} = t_{\text{queue}} + t_{\text{embed}} + t_{\text{sample}} + t_{\text{quantum}} + t_{\text{resolve}} \quad (16)$$

The ‘Classical Execution Time’ for an annealing algorithm consists largely of the ‘post\_processing\_time’, which translates solutions back from the embedded input to match the original input and the ‘qpu\_access\_overhead time’ to compute the total classical execution time as defined in [Equation 17](#). For small problems, this time is typically insignificant but can grow rapidly with problem size.

$$t_{\text{classical}} = t_{\text{post\_process}} + t_{\text{access\_overhead}} \quad (17)$$

For QA, the cumulative times reported in [Figure 2](#) reflect measurements of  $t_{\text{quantum}}$  for increasing anneal times, as specified on line 6 of the benchmarking code. The  $t_{\text{elapsed\_quantum}}$  metric includes all the time needed to perform the annealing operation and obtain a final sample set. This is comparable

to the cumulative times in QAOA. To illustrate the difference between the two, we visualize the data in a slightly different style, where each bar representing a different anneal time has a small vertical offset from the one before it to convey that it represents the time starting at 0. See [section V E](#) for a presentation of these metrics collected from execution on quantum annealing hardware.

## V. EXECUTION ON QUANTUM HARDWARE

Here, we review results obtained from executing our Max-Cut benchmark on two gate model quantum computer systems and a quantum annealing system. The use of multiple quantum technologies positions the benchmark framework as a practical means to quantify the performance of different architectures and to evaluate the effects of modifying algorithm parameters such as rounds, shots, annealing times, and sample size on improving solution quality. Particular emphasis is placed on the quality vs time trade-off in the context of execution on quantum hardware. We use one of the systems to illustrate how total time can be reduced through the use of a containerized execution environment and with parameterized circuit execution.

Note that, apart from the purely quantum computation, the quality of solutions returned by QAOA depends significantly on the quality of classical computations, such as compilation and optimization of beta and gamma for each round. Similarly, the quality of solutions returned by QA depends on the classical operations of minor embedding and post-processing, in addition to the user parameters that control the quantum computation. In this sense, our benchmark framework should be viewed as a tool for evaluating quantum *system* performance in combination with algorithmic choices, rather than the performance of a standalone circuit.

This effort is not intended as a formal comparison of different quantum systems, as we accessed only a small subset of those available. Our tests use default support software and parameter settings provided by the respective manufacturers. Together with the quantum systems themselves, these software tool sets are developing rapidly; therefore, our conclusions about quantum system performance represent a snapshot of progress over time and should not be considered definitive. It is our hope that users will take advantage of the software provided and execute these benchmarks on devices to which they have access, and use them to draw their own conclusions.

### A. Considerations

A number of critical factors may impact the results obtained from running benchmark algorithms on the current generation of quantum computing hardware. We briefly describe these and their impact on the effectiveness of our implementation.

*a. Noisy Hardware* Quantum computers are prone to multiple sources of error. The measurement distribution obtained after executing a quantum circuit on hardware may differ significantly from an ideal system, as circuits become wide and deeper, due to gate infidelity and decoherence. These errors

accumulate in an iterative algorithm such as QAOA and can yield poor result quality. For QA, noise occurs in the form of thermal energy and fluctuations in analog control lines, which can move the qubit particle process out of the ground state.

*b. Native/Physical Gate Set* Quantum circuits can be created with any number of unitary operators, measurements, or gate resets available in quantum computing APIs. Real quantum hardware typically supports a subset of these gates which depends on the type of hardware and its native gate set. A circuit that uses non-native gates needs to be decomposed into natively supported gates using a classical computation process called transpilation, which can be costly for larger circuits. For QA an analogous consideration is the generality of the native Hamiltonian defined in [Equation 7](#); it is an open question whether implementing a more general alternative would have any effect on performance in practice [67].

*c. Device Topology* Multi-qubit gate error depends on the topology of the quantum hardware. Ion trap devices generally support all-to-all connectivity with high fidelity, although this can increase execution time. Superconducting devices, while faster in execution, typically support only nearest-neighbor connectivity. With QAOA, a costly transpilation pass may be required to map multi-qubit logical gates to physical gates by swapping the state between several neighboring qubits appropriately. Topology is also a significant factor in QA computations, for which limited qubit connectivity (number of couplers per qubit) can create challenges for minor embedding and affect the quality of results returned by the quantum processor.

*d. Shared and Remote Access* Quantum computers are expensive, limited in number, and typically shared by many users. Programs can wait in a queue for a long time before being executed, seriously impacting iterative algorithms that require multiple executions of small circuits to converge to a result. Cloud-based access can introduce additional delays when data are transferred between the quantum processor and a classical processor controlling the application.

The sections below illustrate how these factors combine to degrade the quality of the results and lengthen the execution time of hybrid quantum programs executed on hardware (compared to results on a classically implemented quantum simulator as in [section IV C](#)). For example, with more than a small number of qubits, on noisy quantum hardware, the QAOA algorithm may fail to converge to a minimally optimal solution after up to as many as 30 iterations.

## B. Execution on Shared Quantum Hardware

We first show results from executing the Max-Cut benchmark on a remotely accessed gate model quantum computing system that uses ion trap technology. This system is publicly available and shared by multiple users and was chosen to illustrate how the iterative nature of a hybrid quantum-classical algorithm can result in a particularly long time being taken to complete execution and arrive at a solution.

Each parameterized instance of the ansatz circuit is submitted and placed into a queue before execution, and the hybrid application must wait until it completes before proceeding to

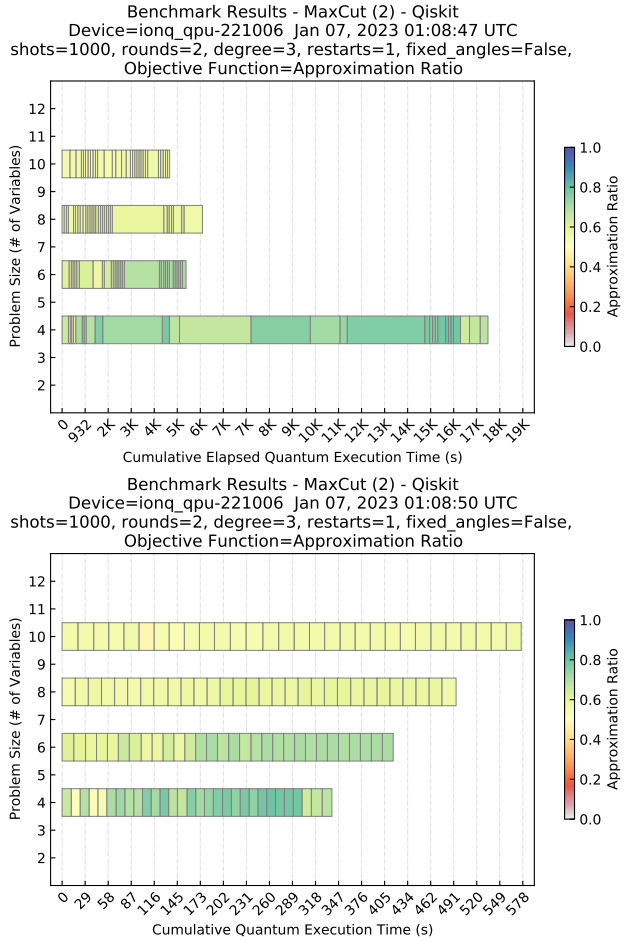


**FIG. 9: Cumulative Elapsed and Quantum Execution Time on Quantum Hardware.** The first plot shows the total elapsed time for executing the Max-Cut benchmark on problems ranging from 4 to 10 variables (4 to 10 qubits) using 30 iterations, each with 1000 shots, on the IonQ Harmony QPU. While inclusive of queue, transpile, load, and quantum execution times, the bulk of the elapsed time is a consequence of a long and variable wait in the queue (e.g.,  $\sim 17000$ s at 4 qubits). This is something that all users will face without privileged access or a containerized execution environment (section V C). The second plot shows only the quantum execution time as reported by the quantum processor and consists of the initialization time and the time taken to execute 30 iterations of 1000 shots on the quantum system ( $\sim 570$ s at 10 qubits). Note the difference in time scales and the increase in execution time for larger problem sizes due to deeper ansatz circuits. (Data collected via cloud service.)

the next iteration. From the benchmark data collected during execution, we are able to factor out the queue time and examine only the quantum execution time, enabling a study of time taken and the quality of result that can be obtained on this class of system, irrespective of queue time.

In Figure 9, we present results from executing the Max-Cut benchmark on problems ranging from 4 to 10 variables (4 to 10 qubits) on the IonQ Harmony QPU, using 30 iterations of 1000 shots each. The first plot shows the total elapsed time (Cumulative Elapsed Quantum Execution Time), i.e., the total of the queue, transpile, load, and quantum execution times

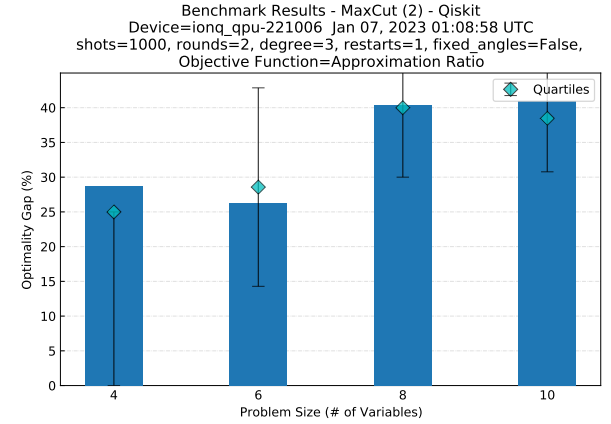


**FIG. 10: Final Optimality Gap.** The optimality gap achieved after the final iteration is displayed for a benchmark run using 2 rounds and 1000 shots for each of four qubit widths (problem sizes) on the IonQ Harmony QPU. (Data collected via cloud service.)

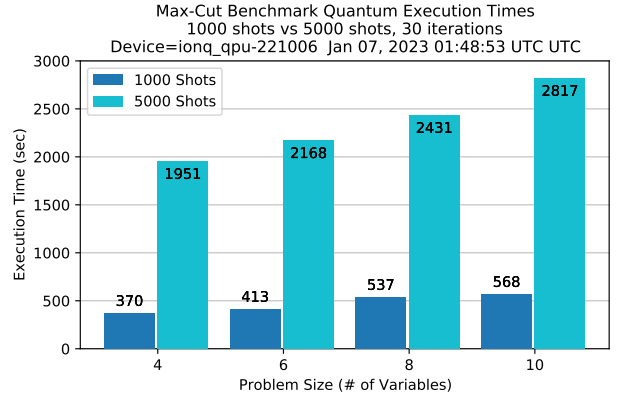


**FIG. 11: Execution Time Increase with Shots.** The quantum execution time for benchmark runs at 1000 and 5000 shots is displayed for each of four qubit widths (problem sizes) on the IonQ Harmony QPU. The height difference between the bars at a specific problem size represents time spent executing an additional 4000 shots over 30 iterations, as both runs share the same initialization time. E.g., at 6 qubits, the execution time per shot can be computed as  $(2168 - 413)/(4000 * 30)$  or  $\sim 14.6$  ms/shot. Increasing shot count as a way to improve solution quality can dramatically increase execution time. (Data collected via cloud service.)

across all iterations (Equation 12). The bulk of this time is a consequence of long wait times in the queue (e.g.,  $\sim 17000$  secs at 4 qubits), which all users will face without privileged access or a containerized execution environment (section V C). The second plot shows the cumulative total of only the quantum execution time (Cumulative Quantum Execution Time) as reported by the system provider via the Qiskit API. The quantum execution time is comprised of the initialization time and the time taken to execute the specified number of shots, in this case, 1000, on the quantum processor (Equation 11).

The quality of the results obtained with a QAOA Max-Cut algorithm is commonly computed as the approximation ratio, as defined in section IV C. From this, we compute the measure

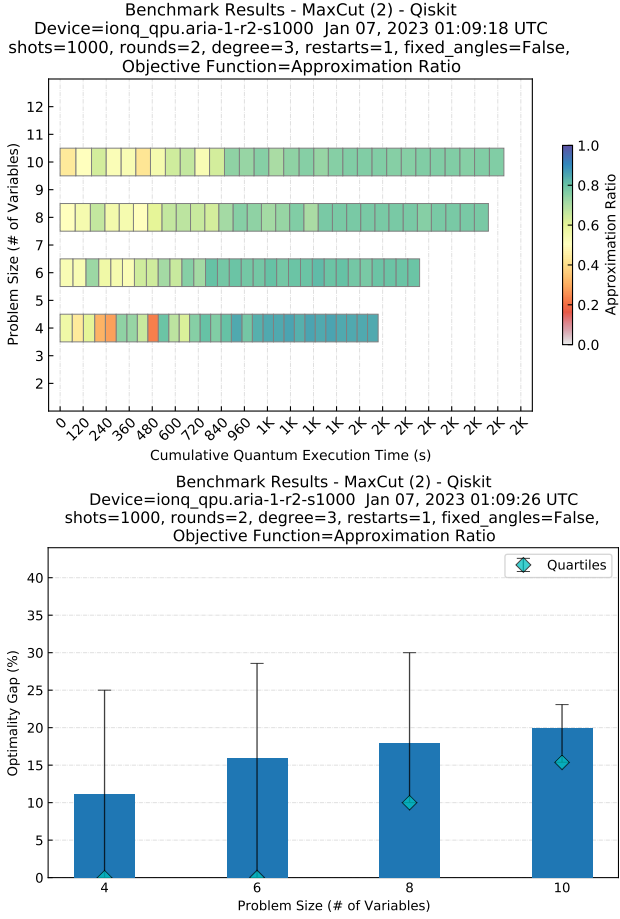


FIG. 12: **Quantum Execution Time and Optimality Gap on IonQ Aria System.** This plot shows the cumulative quantum execution time (~ 2400s at 10 qubits) for executing the Max-Cut benchmark (30 iterations, each with 1000 shots) on the IonQ Aria QPU. The optimality gap seen for this system is improved over the IonQ Harmony System, but the execution time is about 4 times longer. (compared to ~ 570s at 10 qubits on IonQ Harmony). (Data collected via cloud service.)

relevant to optimization specialists, the optimality gap as defined in that same section. Figure 10 shows the final optimality gap computed at the end of execution for each of the problem sizes tested (qubit widths). Note that, above 6 qubits, noise in the quantum system limits the ability of the optimizer to converge to a better result.

Figure 11 illustrates how total quantum execution time is impacted as the number of shots is increased. The benchmark was executed twice, once with 1000 shots and again at 5000 shots. The height difference between the bars at a specific problem size represents the difference in time spent executing an additional 4000 shots over 30 iterations since both runs share the same initialization time. This enables one to compute the execution time per shot for this quantum computing device. E.g., at 6 qubits, the execution time per shot can be computed as  $(2168 - 413)/(4000 * 30)$  or 14.6 ms/shot. This illustrates how increasing shot count as a way to improve solution quality can dramatically increase execution time.

In Figure 12, we present results from executing the Max-Cut benchmark (30 iterations of 1000 shots each) on the IonQ Aria QPU, a second-generation ion trap computer. The first plot shows the cumulative quantum execution time of ~ 2400 secs for 10 qubits. This execution time is about 4 times longer than on the first gen IonQ Harmony System (~ 570 secs for 10 qubits), but the quality of the results is improved, as seen in the optimality gaps shown in the second plot. We did not investigate for this paper the reasons behind the increased execution time and improvement in quality.

### C. Containerized Execution (Co-Location)

As seen in the example above, execution of an iterative QAOA algorithm on a shared quantum computer, accessed through a cloud-based service, can result in very long queue times and added delay due to network data transfer. In this section, we show that total elapsed execution time can be significantly reduced using a containerized execution environment, such as the Qiskit Runtime service provided by IBM Quantum [87] or the Amazon Braket Hybrid Jobs service [88].

Containerized execution environments prevent queue times from being accumulated for each execution of a quantum ansatz in a hybrid quantum-classical program. A complete program, including the classical loop over multiple quantum executions, is uploaded to a provider’s server. An API call initiates execution, and the program is placed in a queue just as a single quantum circuit would be. When the program runs, each quantum circuit execution is performed immediately without waiting again in the queue. The program job continues to execute until it completes, an error occurs, or a maximum execution time is exceeded. This approach offers advantages for users who do not have privileged access to reserve quantum hardware for a series of executions. An added benefit is reduced data transfer latency between the classical portion of the program and the quantum hardware since the classical and quantum processors are typically co-located.

In this model, hybrid program execution is controlled using a network communication interface or API, placing constraints on the structure of programs that can be supported. For example, program data may not be written to a file, but instead are returned via the communication interface. To enable the execution of the Max-Cut benchmark program, it was necessary to develop a control script that modifies small parts of the benchmark code and assembles a container-ready program artifact. A supervisory program uploads the artifact, executes the program, stores returned data to files, and generates plots showing benchmark results. Figure 13 shows the workflow used to execute the benchmark on the Qiskit Runtime service.

In this paper, we used the Qiskit Runtime service to illustrate the execution of the Max-Cut benchmark on a superconducting quantum computing system that supports execution within a containerized environment. This enables us to quantify the improvement in performance that can be achieved through the use of this feature.

Figure 14 shows the total elapsed time (~ 170s at 16 qubits)

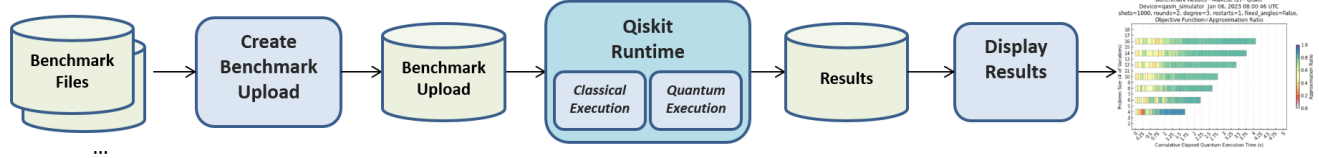


FIG. 13: **Qiskit Runtime Implementation** The diagram illustrates how the benchmark suite is configured to execute within the Qiskit Runtime containerized execution environment. The files that comprise the Max-Cut benchmark are concatenated to produce a single python file, `maxcut_runtime.py`, which is uploaded to the Runtime service. The Qiskit Runtime service controls the tightly coupled execution of both the classical and quantum parts of the algorithm to produce a result record that is returned to the benchmark program for analysis and plotting.

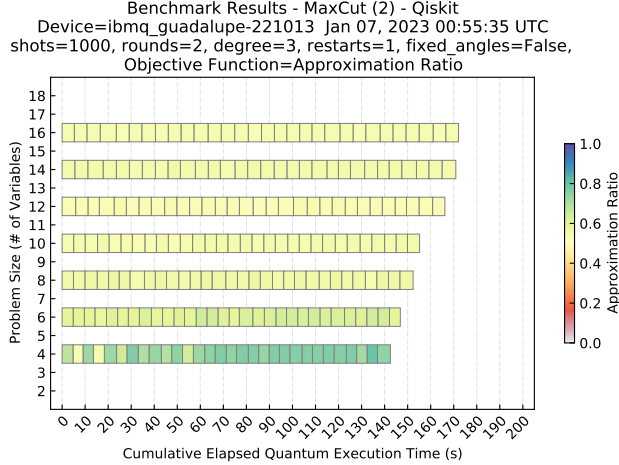


FIG. 14: **Cumulative Elapsed Quantum Execution Time using Containerized Execution.** This plot shows the total elapsed time (~ 170s at 16 qubits) for executing the Max-Cut benchmark (30 iterations, each with 1000 shots) on the IBM Quantum Guadalupe system, inclusive of queue, transpile, load, and quantum execution times. Note that the elapsed time increases regularly as there is no queue time occurring between iterations. The entire run-time job waits in the queue for execution, but once launched, there is no queue time between individual iterations. (Data collected via cloud service.)

for executing the Max-Cut benchmark (30 iterations, each with 1000 shots) on the IBM Quantum Guadalupe system, inclusive of queue, transpile, load, and quantum execution times. Note that the elapsed time increases regularly as there is no queue time occurring between iterations. The entire run-time job waits in the queue for execution, but once launched, there is no queue time between individual iterations. (The initial queue time is not captured or shown in this plot.)

The quality of the results obtained with a QAOA Max-Cut algorithm is commonly computed as the approximation ratio, as defined in [section IV C](#). From this, we compute the measure relevant to optimization specialists, the optimality gap as defined in that same section. [Figure 16](#) shows the final optimality gap computed at the end of execution for each of the problem sizes tested (qubit widths). Note that, above 6 qubits, noise in the quantum system limits the ability of the optimizer to converge to a better result.

[Figure 17](#) illustrates how total quantum execution time is

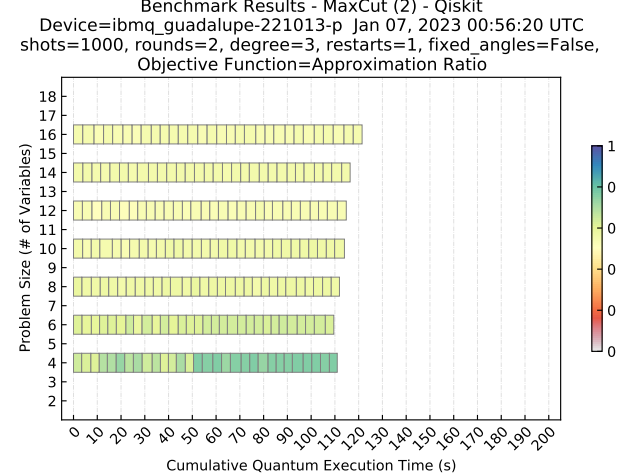
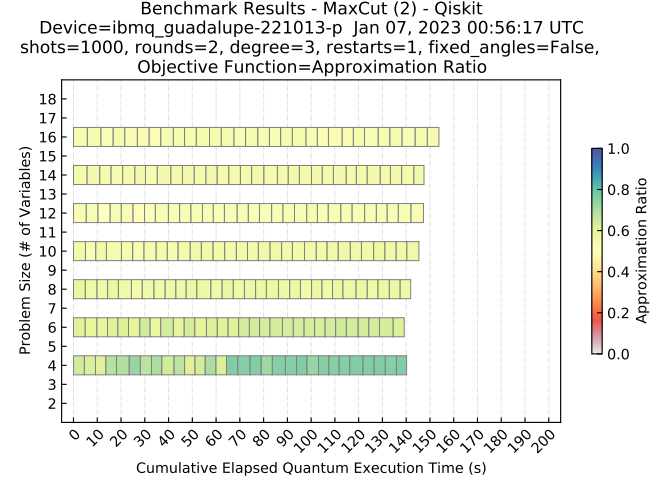


FIG. 15: **Execution Times using Parameterized Circuits.** The first plot shows the total elapsed time (~ 153s at 16 qubits) for executing the Max-Cut benchmark (30 iterations, each with 1000 shots) on the IBM Quantum Guadalupe system using parameterized execution. The reduction from the ~ 170s seen with non-parameterized execution is achieved by eliminating the transpilation of the ansatz circuit prior to each execution by passing parameters to an already transpiled circuit. The second plot shows only the quantum execution time as reported by the quantum processor and consists of the initialization time and the time taken to execute 30 iterations of 1000 shots on the quantum system (~ 122s at 16 qubits). (Data collected via cloud service.)

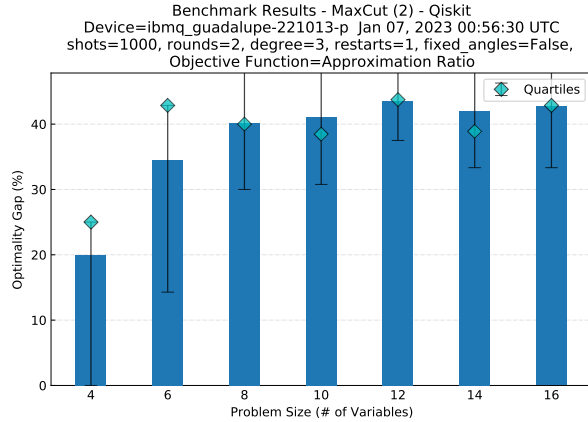


FIG. 16: **Final Optimality Gap.** The optimality gap achieved after the final iteration is displayed for a benchmark run using 2 rounds and 1000 shots for each of four qubit widths (problem sizes) on the IBM Quantum Guadalupe system. (Data collected via cloud service.)

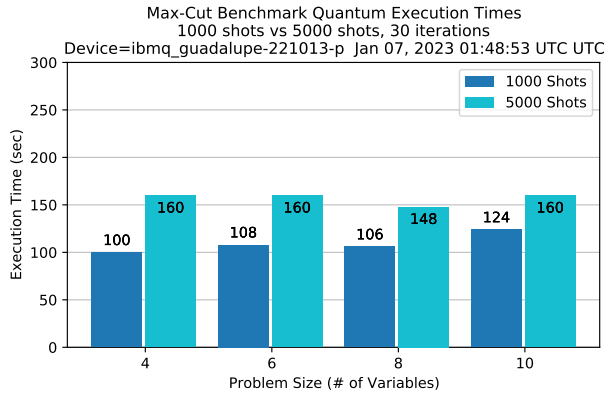


FIG. 17: **Execution Time Increase with Shots.** The quantum execution time for benchmark runs at 1000 and 5000 shots is displayed for each of four qubit widths (problem sizes) on the IBM Quantum Guadalupe system. The difference between the bars at a specific problem size represents time spent executing an additional 4000 shots over 30 iterations, as both runs share the same initialization time. E.g., at 6 qubits, the execution time per shot would be computed as  $(160 - 108)/(4000 \times 30)$  or 0.43 ms/shot. (Data collected via cloud service.)

impacted as the number of shots is increased. The benchmark was executed twice, once with 1000 shots and again at 5000 shots. The height difference between the bars at a specific width (problem size) represents the difference in time spent executing an additional 4000 shots over 30 iterations since both runs share the same initialization time. This enables one to compute the execution time per shot for this quantum computing device. E.g., at 6 qubits, the execution time per shot can be computed as  $(160 - 108)/(4000 \times 30)$  or 0.43 ms/shot.

#### D. Effect of Circuit Parameterization

Another quantum computing feature that can influence the total run time of hybrid quantum-classical applications is the ability to execute parameterized circuits. In the non-parameterized approach, a user must build a circuit, transpile, and bind parameters at each iteration. This can be redundant as the actual circuit does not change from each iteration apart from parameter values for the gates. Using parameterization, it is only necessary to build and transpile the quantum circuit one time at the start of an iteration sequence and efficiently bind newly computed parameter values at subsequent iterations. Here, we illustrate how the Qiskit parameterized circuit capability can improve the overall execution time of the Max-Cut benchmark.

Circuit optimization and transpilation is a classical process used to properly map a circuit to hardware-specific topology and gate limitations, which can be computationally expensive. For the purposes of benchmarking, this time is included as a component of  $t_{elapsed\_quantum}$ , the elapsed quantum execution time, as it is essential to preparing a quantum circuit for execution on a specific hardware system.

The effect of parameterization can be seen by comparing Figure 14, which uses non-parameterized execution, with Figure 15 in which the Qiskit parameterized circuit feature was used. The reduction from  $\sim 170$ s to  $\sim 153$ s is achieved by eliminating transpilation of the ansatz circuit prior to each execution and passing parameters to an already transpiled circuit in subsequent iterations. The second plot shows only the quantum execution time as reported by the quantum processor and consists of the initialization time and the time taken to execute 30 iterations of 1000 shots on the quantum system ( $\sim 122$ s at 16 qubits). Circuit parameterization has no effect on quantum execution time, which represents the execution of the already transpiled and bound circuit on the backend quantum computer.

#### E. Execution on Quantum Annealing Hardware

The QED-C benchmark suite has been enhanced to enable the execution of some benchmarks on backend systems implemented using quantum technologies other than gate model quantum circuits. In this section, we describe the execution of the Max-Cut benchmark on a D-Wave Advantage system, accessed through LEAP Solver “advantage\_system4.1”, as a way to illustrate the framework’s support for test orchestration with varying parameters, capture of relevant performance metrics, and presentation of results in a consistent fashion.

The approach to solving an optimization problem with a quantum annealing device is similar to that used in gate model systems in that a Hamiltonian describing the problem is embedded into the quantum components of the device and evolved in time to settle to the lowest energy state, representing an optimal solution. However, as seen in the description of the benchmark algorithms for the Max-Cut problem, in section IV A, there is a key difference in how the time-dependent evolution is monitored and how the quality vs time trade-off is evaluated.

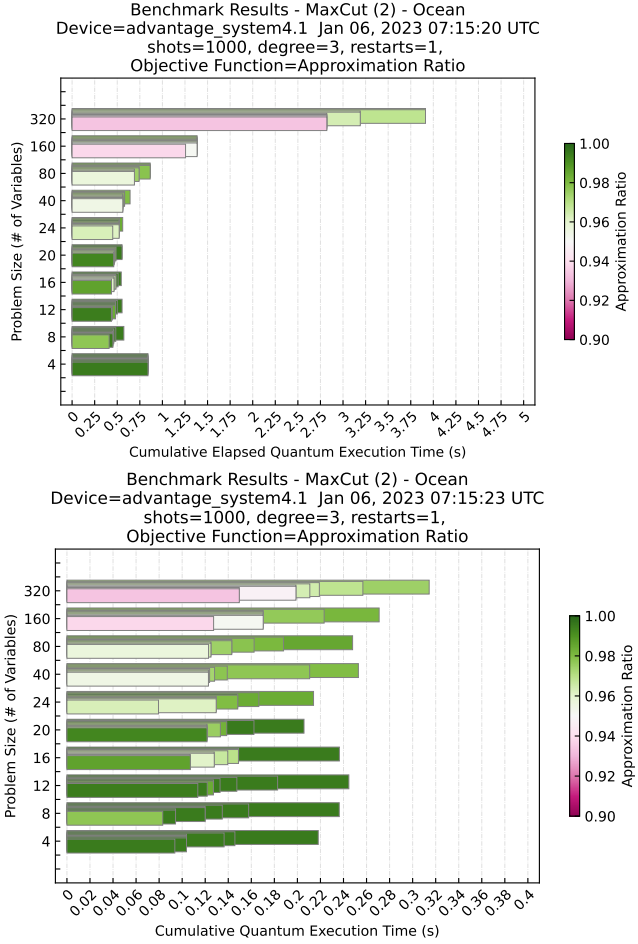


**FIG. 18: Execution on Quantum Annealing Computer.** Here we show results from executing the Max-Cut benchmark program on a Quantum Annealing device. The first plot shows the cumulative elapsed time, and the second shows the cumulative execution time only. The elapsed time includes the quantum execution time as well as data collection and communication between the classical and quantum processors. Under current pricing schemes, the monetary cost of using the QA system is tied to quantum execution time. (Data collected via cloud service.)

A gate model device iterates through a series of quantum circuit executions testing parameter values to find a set that yields a low energy state. In contrast, a quantum annealing system attempts to reach its lowest energy state gradually as a transverse Ising model undergoing quantum mechanical evolution. Comparing the evolution of the state over time in these systems requires that data are collected and presented differently.

In the gate model plots of Figure 9, state evolution is illustrated using a series of rectangles, representing the accumulation of time as each iteration is performed. In Figure 18, the evolution of the quantum state on the annealing device is presented with a single rectangle whose horizontal width represents the time taken to complete a quantum annealing operation, according to a specific annealing time, which we vary from 1 to 128  $\mu$ s. Note that the elapsed quantum execution time shown in the first plot,  $t_{\text{elapsed\_quantum}}$ , includes the time for

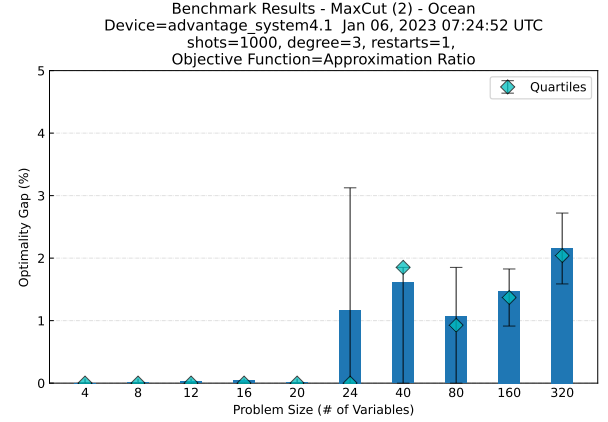


**FIG. 19: Optimality Gap on Quantum Annealing Computer.** This plot presents the final optimality gap at each of the problem sizes tested. (Data collected via cloud service.)

queuing, operations associated with minor embedding (once per job), and executing the annealing process, as described in section IV C. The time shown thus includes more than simply the quantum execution time,  $t_{\text{quantum}}$  (which itself includes the non-quantum operations of chip programming and readout), shown in the second plot.

In the annealing plots, the rectangles are drawn overlaid, representing that evaluation of the annealing process is done by re-executing from the beginning each time, but with varying annealing times. This is done to illustrate the quality vs time trade-off for quantum annealing in a manner that is similar to that of the gate model presentation but unambiguously conveys the differences between the benchmarked algorithms. The intent is to permit a user to quickly see the level of quality that can be expected for a specific annealing time, important in evaluating the overall cost of the quantum annealing solution.

Figure 19 shows the final optimality gap achieved when the annealing process is left to execute for the maximum annealing time of 128  $\mu$ s. For QA and the simple Max-Cut example, the classical computation time involved in performing the optimization is minimal, even for the larger numbers of qubits. However, more complicated optimization problems may require additional classical computation, and the benchmarking framework provides the means to capture and present this additional and important metric to evaluate the total cost of the solution.

## F. Discussion of Hardware Results

The focus of this paper has been on demonstrating the addition of a benchmark based on quantum algorithms for solving combinatorial optimization problems and the framework developed to support this within the existing QED-C benchmark suite. This work is not intended to provide comprehensive comparisons of available quantum computing systems. There are too many variables that contribute to both the quality of the solution and to the total run time for these results to be viewed as a definitive characterization of the systems' performance. A

number of these variables are discussed below in [section VI](#).

For example, by necessity, our tests incorporate two distinct algorithms, QAOA and QA, to match their respective gate model and annealing-based hardware paradigms. These heuristics have different properties and structures, which can significantly affect both computation time and solution quality. This can obfuscate the effects of hardware and system performance. In particular, QAOA incorporates an extra step to optimize the algorithm parameters ( $\beta, \gamma$ ) in each round, which tends to dominate runtime, independent of the platform on which it runs. Our tests do not explore possible improvements to the default algorithm offered by one manufacturer or algorithmic improvements in the classical optimizer, defaulting to the open-source implementation of COBYLA [89]. We do not execute on the latest-available hardware, nor do we investigate error mitigation strategies that may be already incorporated in some hardware systems.

For all of these reasons, we caution readers that using these incomplete results to draw general conclusions about hardware performance alone would likely be misleading. A full-scale study of all these factors contributing to performance, to tease out the hardware contribution, is beyond the scope of the paper.

Quantum computing hardware is expected to rapidly evolve with improvements in fault tolerance and error correction. We believe that as these machines evolve, more focused versions of the benchmark we have illustrated here will be critical to gauging the concomitant improvement in performance. Some examples of this approach, which focus on specific aspects of the computation, are presented in the next section.

## VI. RESULT QUALITY AND HYPER-PARAMETERS

The performance of an optimization algorithm is often studied in terms of the trade-off between the quality of the obtained result, and the resources required to achieve it. In many real-world applications, a high-quality result is required within a limited amount of time. It is desirable to predict in advance whether it is possible to obtain a solution with acceptable quality within the available time budget and to determine the parameter values that result in high-quality outputs.

However, a large number of options (or “hyper-parameters”) can be used to control the execution of QAOA, and it is important that conclusions not be drawn from just one set of results, obtained with limited exploration. Furthermore, metrics other than the approximation ratio can also be used to assess result quality, which we discuss in this section. While various hyper-parameters, such as the number of shots, choice of the classical optimizer, number of iterations, and rounds, affect result quality, we focus on the effects of values of initial angles on the performance in this section. We end this section with a discussion of a parameter tuning strategy to help identify good hyper-parameters for QAOA execution. (Similar strategies can be developed for QA, although it is not discussed here.)

While this section refers to QAOA in the context of the Max-Cut problem, most of the conclusions hold more generally for QAOA. Throughout this section, we use the terms cut size and (the negative of) energy interchangeably, where energy refers

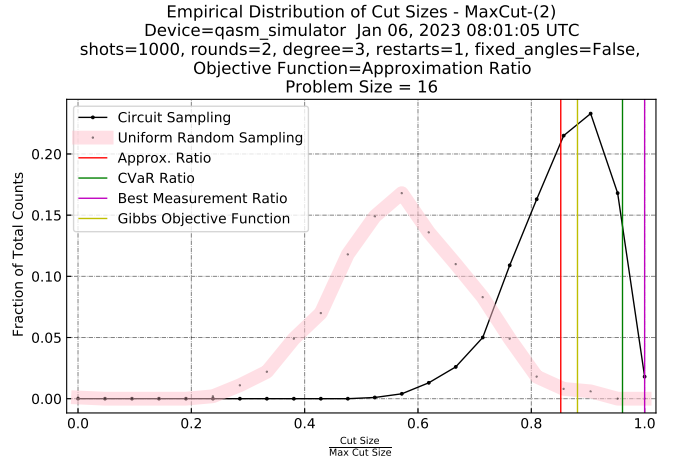


**FIG. 20: Cut Size Distribution:** The quality of the final output of QAOA can be understood by inspecting the distribution of the cut size values obtained at the final optimizer iteration. A distribution peaked closer to the right indicates higher result quality. Also plotted here are the various metrics (vertical lines), and the distribution corresponding to a uniform random sampling of bit-strings (pink line).

to the eigenvalues of the Hamiltonian in [Equation 4](#).

### A. Result Quality and Objective Functions

Here, we discuss the role of the approximation ratio and other related metrics in quantifying result quality, as well as various choices for the objective function. The benchmarking framework generates optimality gap plots and cut size distribution plots as effective tools to succinctly visualize these additional metrics.

We recall that (iterative) QAOA comprises two tasks: (a) sampling from a parameterized quantum probability distribution (handled by the QPU), and (b) finding parameter values that maximize a function of the observed distribution (handled by the optimizer routine). While the optimizer is usually tasked with maximizing the approximation ratio, we emphasize that the final output of QAOA is not the approximation ratio, but the best-measured cut (i.e., the cut corresponding to the largest cut size) obtained across all iterations of the algorithm.

A reasonable measure of result quality should take into account the probability distribution of cut sizes (illustrated in [Figure 20](#)), as explained below. The approximation ratio, for example, is proportional to the mean of the measured cut sizes of the distribution. Hence, parameter values (i.e., angles) that result in a significant proportion of measured shots having small values of cut sizes (compared to the optimal) produce a low approximation ratio. Although the best-measured cut as a measure of result quality is often a poor metric because of being numerically unstable, it has inspired a few other objective functions. Two of these, the Conditional Value at Risk or CVaR [90], and the Gibbs objective function [91] focus on the tail end of the distribution, rather than treating all measurements equally.

These objective function metrics are defined as follows. Let

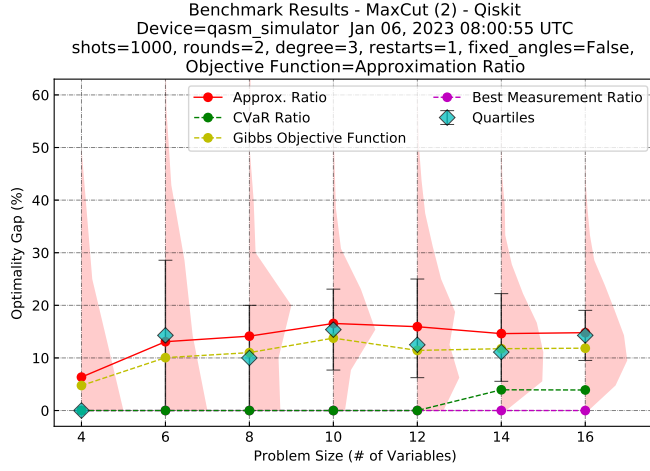


FIG. 21: **Detailed optimality gaps plots.** A variety of metrics can be used to assess the quality of the final distribution of outputs of QAOA. For each implemented problem size or circuit width (along the X-axis), we plot the optimality gap (along the Y-axis). The obtained distributions of optimality gaps are shown as pink half-violin plots. The optimality gap values in terms of the CVaR ratio, approximation ratio, Gibbs Ratio, and Best Cut ratio are shown as line plots.

$M$  denote the number of shots, so that for given values of (vectors)  $\beta, \gamma$ , we obtain  $M$  cut-sizes, one corresponding to each of the bit-strings obtained from computational basis measurements. Let these energies be denoted by  $E_1, \dots, E_M$ , arranged in non-decreasing order. Note that since these energies are  $\leq 0$ ,  $|E_1|, \dots, |E_M|$  are non-negative integers arranged in non-increasing order. Then, the energy expectation value is approximated by

$$F \approx \frac{\sum_{i=1}^M E_i}{M}. \quad (18)$$

On the other hand, CVaR [90], for a chosen value of parameter  $\alpha \in (0, 1]$  is defined as

$$\text{CVaR}_\alpha(\beta, \gamma) = \frac{1}{\lceil \alpha N \rceil} \sum_{i=1}^{\lceil \alpha N \rceil} E_i, \quad (19)$$

where  $\lceil \cdot \rceil$  denotes the ceiling function.  $\text{CVaR}_\alpha$  denotes the mean value of (the negative of) cut-sizes over the lower  $\alpha$ -tail of the distribution of measured energies. The limit  $\alpha \rightarrow 0$  corresponds to the ground state energy value (i.e.,  $E_1$ ), while  $\alpha = 1$  corresponds to the energy expectation value  $F_{\beta, \gamma}$ . The value of the metric depends on the choice of  $\alpha$ . While the value of this parameter can be configured, we default to  $\alpha = 0.1$  in all plots and analyses.

Another choice is the Gibbs objective function [91], which is defined as

$$f_\eta(\beta, \gamma) = \ln \langle \beta, \gamma | e^{-\eta H} | \beta, \gamma \rangle, \quad (20)$$

for  $\eta > 0$ , and where  $H$  denotes a Hamiltonian whose ground state is sought. The parameter  $\eta$  determines the relative weights of the low energy states of  $H$  in the expression. The parameter  $\eta$  tunes  $f_\eta$  between two extreme values (similar to  $\alpha$  in

$\text{CVaR}$ ):  $f_{\eta=0}(\beta, \gamma) = F_{\beta, \gamma}$ , while  $f_{\eta \rightarrow \infty} = E_{\min}$ , i.e., the lowest measurable energy of  $H$  on the state  $|\beta, \gamma\rangle$ .

In our benchmarking framework, the objective function may be set to any of these. It is convenient to normalize each of these objective functions so that they lie in the range  $[0, 1]$ . Hence, we define the following quantities:

$$\begin{aligned} \text{Approximation Ratio } r &= \frac{F_{\beta, \gamma}}{E_{\min}}, \\ \text{CVaR}_\alpha \text{ Ratio} &= \frac{\text{CVaR}_\alpha}{E_{\min}}, \\ \text{Gibbs Ratio} &= \frac{f_\eta}{\eta E_{\min}}, \\ \text{Best Measurement Ratio} &= \frac{E_1}{E_{\min}}. \end{aligned} \quad (21)$$

The approximation ratio is commonly used in studies of quantum computing solutions to optimization problems, with the other ratios appearing less often. These are measures of solution quality where a value of 1.0 is optimal. However, within the Operations Research community, quality is more often characterized by the “optimality gap” or percentage distance from optimal. Throughout this paper, the optimality gap is defined in terms of the distance from the optimal objective function, defined as  $(1.0 - \text{approximation\_ratio}) \times 100$  and described in section IV C.

A succinct way of visualizing the quality of the output from the QAOA algorithm is seen in the optimality gap plot in Figure 8 and others. Our framework also generates what we call ‘detailed optimality gap plots’ (e.g., Figure 21). For each problem size, the empirically obtained distribution of cut sizes is shown using a half-violin plot. (The plotted distribution is actually that of the quantity  $1 - \frac{\text{Cut Size}}{\text{Optimal Cut Size}}$ , so that it is normalized to be between  $[0, 1]$ ). The four metrics in Equation 21 are also shown in terms of the optimality gap, i.e.,  $(1 - \text{metric\_value}) * 100$ . This provides a snapshot of the results quality as a function of problem size in terms of various quality metrics.

## B. Initial Angles and Restarts

While a number of hyper-parameters such as rounds, shots, number of optimizer iterations, etc., affect the ability of the iterative QAOA execution to obtain a high-quality output, perhaps the most important and non-trivial choice is that of the initial values of the angles.

The classical optimizer routine faces a number of challenges. Finding the optimal angles for QAOA has been shown to be an NP-HARD problem [83]. Additionally, the landscape of the objective function suffers from ‘barren plateaus’, a condition where the gradient of the objective function is close to zero, hindering training of the angles [92]. Barren plateaus can also be exacerbated by the choice of objective function [93], noise in quantum hardware [94], or large entanglement in the ansatz [95].

A consequence of these challenges is that the choice of the initial angles (i.e.,  $\beta$  and  $\gamma$ ) can substantially impact the ability

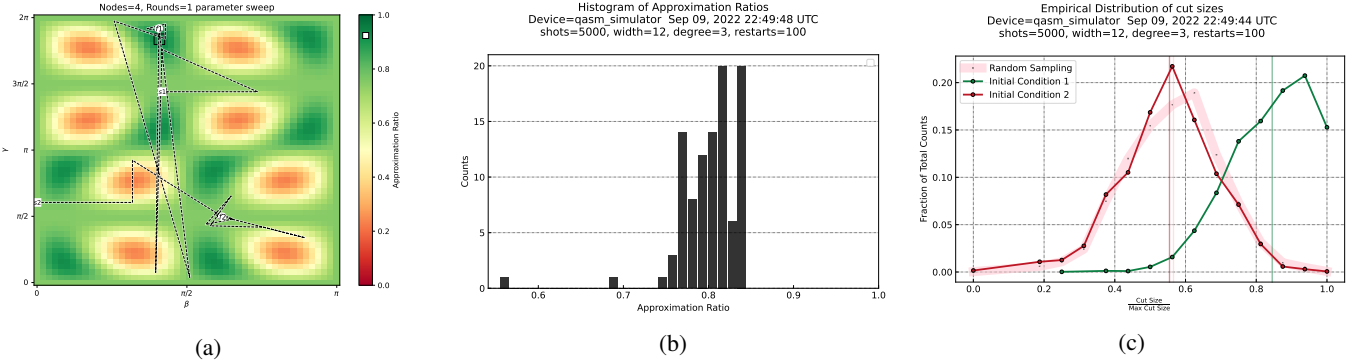


FIG. 22: **Values of Initial Angles Affect Result Quality.** (a) *Parameter trajectories and approximation ratio landscape:* The COBYLA optimizer navigates the parameter space differently depending on the initial parameter values. The trajectory taken for two randomly chosen initial angles values (labeled  $s_1$  and  $s_2$ ) is shown in the backdrop of the approximation ratio landscape obtained from state-vector simulation. The parameters at the end of the 30 iterations are labeled by  $f_1$  and  $f_2$ , respectively. (b) *Histogram of approximation ratios* obtained at the end of 30 COBYLA iterations from QAOA simulations for 100 restarts succinctly shows the variability associated with initial conditions. While most restarts result in an approximation ratio between 0.75 and 0.85, some result in a substantially lower approximation ratio. (c) The distribution of cut sizes at the end of 30 iterations for two initial conditions are substantially different, with initial condition 2 almost overlapping with a random sampling of bit-strings, while initial condition 1 results in a relatively high approximation ratio of  $\approx 0.83$ .

of the optimizer to reach the optimal value of the objective function. For example, Figure 22a shows the trajectories of angles probed by the optimizer for two randomly chosen initial angles. The distribution of the cut sizes obtained at the end of 30 optimizer iterations is substantially different, as shown in Figure 22c. While one choice results in an output practically indistinguishable from a random sampling of bitstrings, the other results in a high-quality distribution of cuts. We also plot a histogram of approximation ratios in Figure 22b from one hundred random initializations.

These issues have spurred substantial research for addressing and overcoming these challenges. While many proposals have been put forth, keeping in mind our objective of benchmarking the performance of quantum solutions available to end users, we focus on implementing the most basic approach for mitigating some of these effects. Specifically, we implement multiple ‘restarts’, i.e., we run QAOA multiple times using random angles as initial angles for the optimizer and report the output corresponding to the best restart.

To that end, our benchmarking framework allows the user to specify the number of restarts, through a parameter called `max_circuits`. By default, this parameter is set to one, and all the initial  $\beta$  and  $\gamma$  angles are set to 1. Thus, all the results in section V use these angles as the starting angles. For restarts  $> 1$ , for each problem size, the output corresponding to the best restart is displayed in the plots. Figure 23 shows the output corresponding to 10 restarts for the same parameters as Figure 8. The results quality is noticeably better for the smaller problem sizes. The user can also specify initial angles manually, using the `thetas_array` parameter.

### C. Fixed Angle Conjecture

While multiple initializations or restarts mitigate some of the difficulties faced by the optimizer, the cost of implementing the

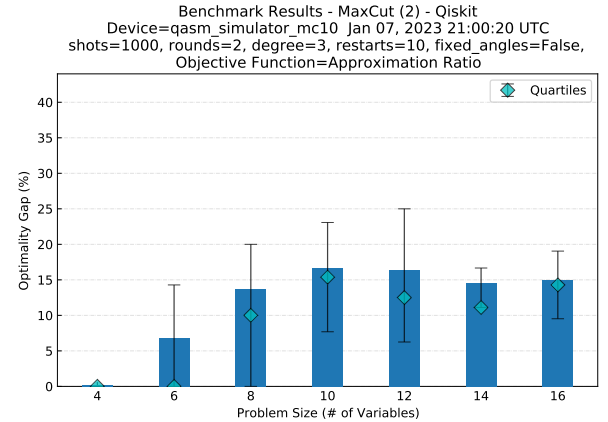


FIG. 23: **Optimality Gap with Multiple Restarts.** Here we show the results obtained when executing the Max-Cut benchmark 10 times at each problem size. The result shown for each of the problem sizes represents the ‘best’ result obtained for that problem size across all 10 restarts, defined as the result showing the highest approximation ratio.

optimizer routine multiple times can be substantial, requiring many-fold \*quantum) processing unit access time.

A recent study [96] proposes an optimization-free QAOA implementation, by executing the ansatz for each problem only once using so-called ‘fixed angles’. The authors show that at these angles, the approximation ratio is higher than the threshold for every problem instance for 3-regular graphs. While these angles are not the global maxima of the approximation ratio landscape, they guarantee close to optimal performance without performing the costly optimizer loop. For example, Figure 24 shows that the optimality gap for all problem sizes (except 4) with fixed angles is practically the same as in Figure 23, which required 10 restarts with 30 optimizer iterations each. This corresponds to a reduction in QPU access time by a

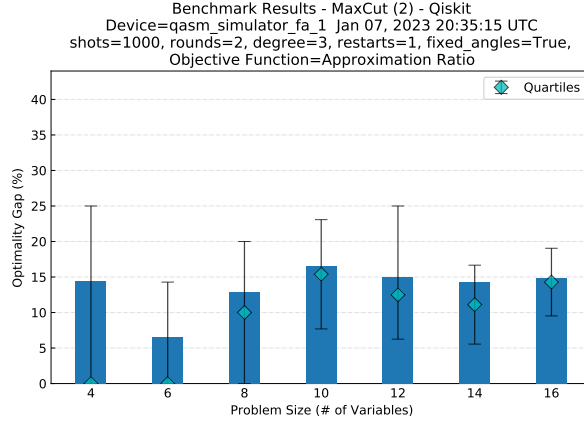


FIG. 24: **Optimization-free QAOA Implementation using Fixed Angles.** To avoid restarts and the costly optimization loop, one may use the ‘fixed angles’ that are guaranteed to result in a good quality output [96]. Shown here is the optimality gap using fixed angles for rounds=2, without implementing the minimizer routine.

factor of  $\approx 300$  while yielding similar quality results.

Hence, the benchmark framework includes a provision for choosing the initial angles to be the fixed angles by setting the `use_fixed_angles` flag to be `True`. The optimizer iterations can simultaneously be set to 1, to not use the optimizer routine.

In Figure 25 we present results from a test that was run using this benchmark feature to explore ‘parameter concentration’ [97]. For problem sizes ranging from 4 qubits to 20 qubits on 3-regular graphs, 100 random initial angles, and run 30 (COBYLA) optimizer iterations each. Shown in this plot are the  $\gamma$  values obtained as final values by the optimizer along with the corresponding approximation ratios. The angles obtained by the optimizer are seen to cluster around four values, most of which match the values proposed in [96]. The choice of initial angles clearly influences the final outcome of the algorithm, and a strategy for the selection of these angles is critical for optimal performance.

#### D. Parameter Selection Strategy

Previously, we showed how the choice of initial angles and number of rounds, shots, and restarts could affect the performance of the QAOA implementation. In addition, the performance could vary from one problem instance to another. These considerations raise the following question: For previously unseen problem instances, can we predict parameter values that are likely to result in the best performance? Specifically, given a notion of resource (e.g., QPU access time) and a metric for result quality (e.g., approximation ratio), what parameter values should be used to get optimal performance given a resource budget?

With that goal in mind, a benchmarking framework for parameterized stochastic optimization algorithms such as QAOA and quantum annealing is being developed in a parallel effort [98]. While this framework [99] is applicable to other algorithms as well, we apply it to the QAOA simulations using

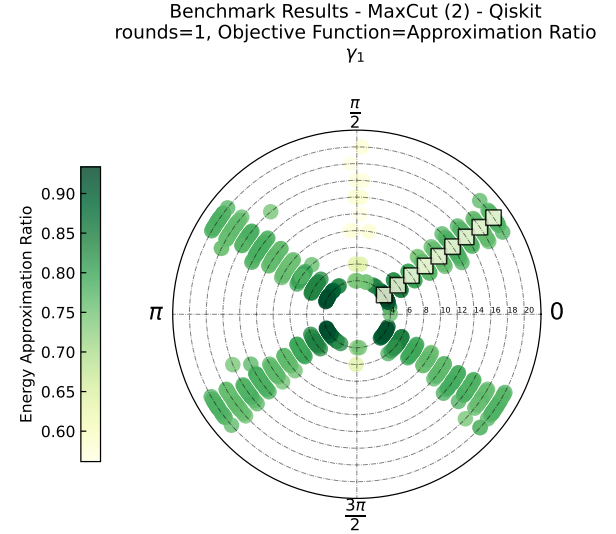


FIG. 25: **Angles cluster around certain values.** For 3-regular graphs with sizes ranging from 4 qubits to 20 qubits, we choose 100 random initial angles, and run 30 (COBYLA) optimizer iterations each. The final values of the angles obtained by the optimizer are seen to cluster around four values. Shown here are the  $\gamma$  values, along with the corresponding approximation ratios.

results obtained from the QED-C benchmarking framework. This framework generates parameter recommendations over a grid of resource values and also plots the corresponding performance compared to the best performance seen in the data.

The input to the framework consists of performance data obtained empirically by implementing an algorithm on a variety of problem instances. The data includes the quality of the result, which we call the performance metric, corresponding to many executions of the algorithm, over a range of parameter value settings. A function is provided to compute the resources expended for each execution.

The framework first splits the problem instances into two sets- a testing set and a training set. A statistical analysis of the training set data is then used to identify parameter values that are likely to lead to high performance when applied to the test set. On the other hand, for each instance in the test set, parameter values as a function of the resource corresponding to the highest result quality found so far are identified from the available data for all resource grid values. These are summarized in the form of a curve we call the ‘virtual best’.

Thus, the parameter values corresponding to the virtual best simulate knowing ahead of time for each instance what the best parameters would be for any resource value. The virtual best provides a bound on the performance that any parameter-setting strategy using the data provided for the analysis can provide. Thus, the recommended parameters and virtual best parameters are plotted together in a ‘strategy plot’. In a separate plot, the virtual best performance is plotted along with the performance obtained on the test set using the recommended parameters.

We now present an analysis of QAOA using this framework.

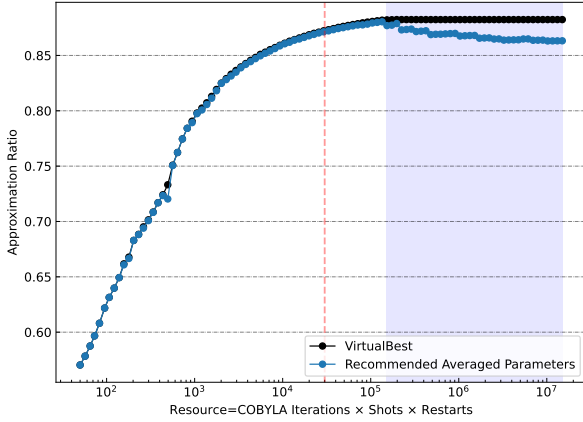


FIG. 26: **Solution Quality vs Total Resource Utilization:** The virtual best provides a bound on the best performance attainable by any parameter strategy. Shown here are the performance profiles of the virtual best, along with the performance obtained from the parameters recommended by the stochastic-benchmarking framework [99]. The red dashed vertical line corresponds to the resource value used throughout the hardware section (30 iterations, 1000 shots, 1 restart). The shaded area highlights the regime, after which the approximation ratio drops with increasing resources.

Figure 26 shows the obtained performance profile, while Figure 27 shows the strategy plots generated by the framework, using an 80%-20% train/test instances split. The QAOA algorithm is executed using noiseless simulations with two rounds for 50 distinct 3-regular graphs of size 12. We implemented runs corresponding to a range of values for restarts  $[1, \dots, 100]$ , number of classical optimizer (COBYLA) iterations  $[1, \dots, 30]$ , and shots  $[50, \dots, 5000]$ . We capture the number of times the processing unit was accessed by defining the resource as the product of these parameters.

Figure 26 can be used to determine the relative performance of the recommended parameter values with respect to the optimistic bound given by the virtual best. In this example, we observe that both lines are almost overlapping, showing that good parameter values are shared across the training (recommended parameter values) and testing (virtual best parameter values) instances. In particular, these results show that with increasing access to the processing unit, the quality of the response increases as measured by the approximation ratio up to a certain point. The shaded area in this figure shows a regime in the resource quantity where the performance metric decreases with increasing resources. This is counter-intuitive and reveals that given the data used to generate this analysis, the best parameter values are given with the COBYLA iterations being set to 30, 100 restarts, and only 50 shots. Combinations of parameter values yielding larger resource usage diminish the approximation ratio. This observation suggests that if allowed more processing unit access, increasing the number of shots deteriorates the performance.

Moreover, it highlights that the number of classical minimizer iterations should be increased before the number of restarts, when more resources become available, always aiming toward keeping the number of shots small. The dashed red

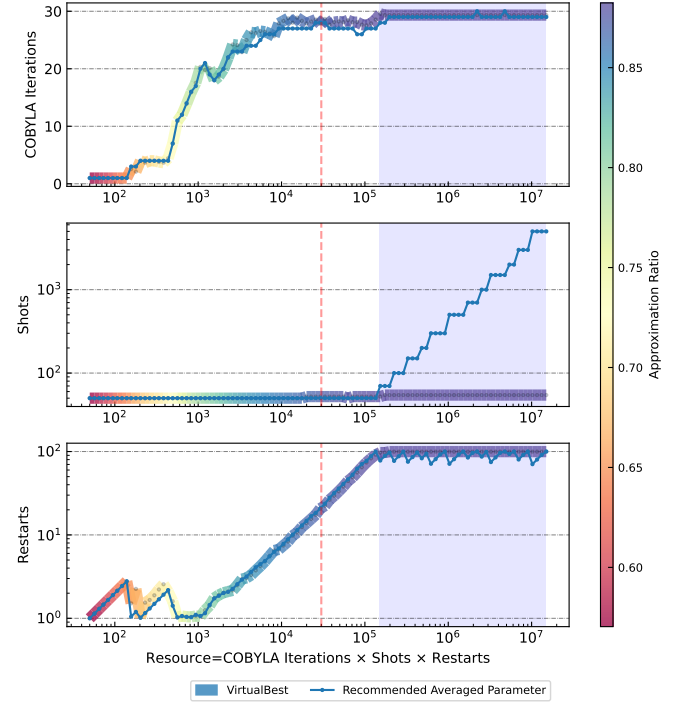


FIG. 27: **Strategy Plots:** For each resource value, the framework recommends values of minimizer iterations, shots, and the number of restarts that are likely to lead to the best performance. For comparison, the virtual best parameters are also plotted as colored curves, with the colors indicating the corresponding approximation ratio. The red dashed vertical line corresponds to the resource value used throughout the hardware section (30 iterations, 1000 shots, 1 restart). The shaded area highlights the regime, after which the approximation ratio drops with increasing resources.

line shows the equivalent resource usage of the simulations in the remaining of section VI. Notice how the recommended parameter values, as seen in Figure 27, i.e., 27 COBYLA iterations, 20 restarts, and 50 shots, are not the same as the ones used in the other experiments, i.e., 30 COBYLA iterations, 1 restart, and 1000 shots. Using this analysis, and specifying a performance metric and a resource function, one can use empirical data to inform parameter setting values. Moreover, these results can also inform about the instances themselves. In this example, the problem instances are relatively small, i.e., 12 node graphs with a solution space of size  $2^{12} = 4096$ . When solving the problem with QAOA, sampling the output distributions extensively with many shots does not lead to as much approximation ratio improvement compared to reinitializing the problem (restarts) or allowing more classical optimization iterations.

These parameter-setting strategy analyses provide practical recommendations for the usage of the algorithms such as the one discussed in this manuscript.

## VII. SUMMARY AND CONCLUSIONS

While the current generation of quantum computers may be limited in computational power, it is expected that these systems will rapidly evolve and become capable of performing increasingly complicated tasks. We believe it is critical to this advancement effort to establish accurate and validated methods for measuring progress that are readily available to the developers of these systems as well as the users who utilize the resource in solving real-world problems.

To this end, we built on the evolving suite of QED-C Application-Oriented Benchmark programs, enhancing it to enable benchmarking of hybrid quantum-classical solutions to combinatorial optimization problems, often cited as a use case for quantum computing. The enhancements apply to both quantum annealing and gate-model quantum computers as a way to demonstrate the platform’s extensibility to a variety of quantum technologies. The framework measures performance characteristics across multiple dimensions and presents results in ways that are easy to understand for new users and in a context familiar to experts in this field.

The techniques developed here can serve as a valuable tutorial about approaching optimization problems in quantum computing, especially in understanding the trade-off between the quality of the solution and the time required to achieve a solution, as well as the limitations of the algorithms. They can highlight what is reasonable to expect when using quantum computing algorithms to address such problems, offering practical guidance for end users by demonstrating the implementation challenges and real difficulties in using these algorithms. Users are able to execute these benchmark programs on devices to which they have access and evaluate for themselves the total cost of ownership of this technology, a key to understanding how and when quantum computers may be able to offer measurable value.

Multiple factors affect the ability of a quantum computer to effectively produce solutions for combinatorial optimization problems. For both quantum annealing and gate-model quantum computers, the algorithms used to find these solutions provide only an approximate answer, and the quality of the results is typically a function of the time available for processing, often under tight constraints.

For gate model computers, a variational algorithm such as QAOA is expensive in terms of time due to its requirement to execute an ansatz circuit multiple times, seeded with an initial set of parameters, to determine the lowest eigenstate from those parameters. While it is known that improved results can be obtained through the use of multiple rounds within a particular ansatz, this requires optimization of additional parameters and increases the length of the circuit. With QA, we provide a mechanism to evaluate how the quality of results is affected by the annealing time allocated, which is related to the total monetary cost of obtaining a solution.

When QAOA is run on hardware, the quality of the result will degrade compared to a simulator, as the programs will be negatively impacted by noise. To illustrate the practical limits to execution on hardware, the benchmarks are executed on three different classes of quantum computer, ion trap, super-

conducting transmon, and quantum annealing system. While it is tempting to present a detailed comparison of the performance of these systems, it is not the goal of this work as we do not execute on all the latest hardware, nor do we select all options that may improve the results. Any comparisons between hardware systems would be incomplete, and it would be irresponsible to draw misleading conclusions given these limitations.

As a general demonstration of the benchmark framework, for gate model devices, we show that the quality of the results is higher using ion trap technology, but the execution is substantially faster on superconducting transmon devices. It is notable that both the quality of the results obtained and the execution time from using a quantum annealing device are better than both gate model examples illustrated above. This may be a consequence of the comparative maturity of the annealing hardware, as well as the fact that quantum annealing is naturally suited for optimization applications, which can use solutions even when they aren’t perfectly optimal.

For optimization as an application area for quantum hardware, consideration should be given to using the QA algorithm and associated hardware (not just QAOA). Whether classical or quantum, hardware that is specialized to one specific algorithm, QA in this case, would be expected to outperform more general hardware that can run any algorithm. However, gate model devices may eventually reach a broader range of applications as quantum error correction enables fault-tolerant computing, given that many gate model algorithms can be applied to problems beyond combinatorial optimization. Current research on QAOA is focused on how to make the approach more sophisticated (e.g., incorporating constraints, rather than minimization of a single energy function). This approach could provide QAOA a competitive advantage over specialized hardware like QA with the co-design of new QC algorithms and ansatz circuits that are specific to particular applications.

We consider this work to be forward-looking with respect to the available technology. The complexity of discrete optimization problems motivates the development of methods, such as QAOA and QA, that may be challenging in the worst-case analysis yet provide value in practice. Performance-based metrics and benchmarking tools can quantify these proposed methods’ progress and provide a way of comparing alternative solutions whose capabilities are beyond those currently available. As quantum computers evolve, the benchmark methods we have defined here will be critical to gauge the improvement in performance.

## CODE AVAILABILITY

The code for the benchmark suite introduced in this work is available at <https://github.com/SRI-International/QC-App-Oriented-Benchmarks>. Detailed instructions are provided in the repository.

## ACKNOWLEDGEMENT

We acknowledge the use of IBM Quantum services for this work. The views expressed are those of the authors and do not reflect the official policy or position of IBM or the IBM Quantum team. IBM Quantum, <https://quantum-computing.ibm.com/>, 2021.

We acknowledge IonQ for the contribution of access to hardware. The views expressed are those of the authors and do not reflect the official policy or position of IonQ.

We acknowledge D-Wave Systems for the contribution of access to both hardware and software tools. The views expressed are those of the authors and do not reflect the official policy or position of D-Wave Systems.

Contributions to this work from Los Alamos National Laboratory were conducted under the auspices of the National Nuclear Security Administration of the U.S. Department of Energy under Contract No. 89233218CNA00001. This research used resources provided by the Los Alamos National Laboratory Institutional Computing Program and was supported by the Laboratory Directed Research and Development program under the project 20210114ER.

D.B. acknowledges NASA Academic Mission Services (contract NNA16BD14C – funded under SAA2-403506). P.S. acknowledges support from the NASA/USRA Feynman Quantum Academy Internship program. Both D.B. and P.S. are supported by NSF Expeditions in Computing program CCF #1918549. This work used computational and storage services associated with the Hoffman2 Shared Cluster provided by UCLA Institute for Digital Research and Education’s Research Technology Group.

Amazon Braket™ is a trademark of Amazon Technologies, Inc. D-Wave®, Ocean™, and Advantage™ are trademarks of D-Wave Systems, Inc. IBM®, Qiskit®, IBM Q® and IBM Quantum System Two™ are trademarks of International Business Machines Corporation. IonQ™, IonQ Harmony™ and IonQ Aria™ are trademarks of IonQ, Inc.

We acknowledge Jerry Gamble of Verizon Corporation for his contribution to code development and editorial efforts on this manuscript. We acknowledge Jason Necaise in the Department of Physics and Astronomy, Dartmouth College (previously with D-Wave Systems), for his contribution to code development.

We thank Mark Johnson (D-Wave), Andrew Wack (IBM), David McKay (IBM), Paul Nation (IBM), Luning Zhao (IonQ), Ananth Kaushik (IonQ), Farshud Sorouimaran (Ohio State University), Amos Anderson (Quantum Circuits), Steve Reinhardt (Quantum Machines), Davide Venturelli (USRA/NASA), Filip Maciejewski (USRA/NASA), and others for providing comments on this manuscript.

## Appendix A: Methods for Combinatorial Optimization

We present a general introduction to the theoretical foundations of combinatorial optimization problems and their implications for developing experiments to study solver performance (a solver is an algorithm or heuristic that has been implemented in software or hardware). The issues discussed here informed our decisions about the choice of inputs and performance metrics in designing the QED-C benchmarking framework.

### 1. Combinatorial Optimization Theory

For concreteness, we consider the class of combinatorial optimization problems defined on  $n$  integer-valued variables  $x = \{x_1, \dots, x_n\}$ , containing  $m$  constraint functions  $c(x)$ , and one objective function  $f$  that is a polynomial in  $x$ , as follows.

$$\begin{aligned} \min : & f(x) \\ \text{s.t.: } & c_i(x) \leq 0 \quad \forall i \in \{1, \dots, m\} \\ & x_i \in \mathbb{Z} \quad \forall i \in \{1, \dots, n\} \end{aligned} \quad (\text{A1})$$

Given a problem thus described, the algorithmic goal is to find an assignment of integer values to  $x$  that obeys all the constraints, and that minimizes the value of  $f(x)$ . For example, this simple problem,

$$\begin{aligned} f(x) &= x_1 + 2x_2 \\ c_1(x) &: -x_1 + 1 \leq 0 \\ c_2(x) &: -x_2 + 1 \leq 0, \end{aligned}$$

asks to find two positive integers that minimize  $f(x)$ ; an optimal solution  $x_1 = 1, x_2 = 1$  has the objective value  $f(x) = 3$ .

This notation is general enough to cover an enormous variety of optimization problems of interest to all sectors of industry. To name just a few:

- The **Job Shop Scheduling** problem and its variations are ubiquitous in industry scheduling problems associated with efficient assignment of multiple resources to multiple tasks.
- The **Portfolio Optimization** problem is of interest to finance. E.g., given a list of items to purchase, select a subset of items to maximize profit and minimize risk.
- The **Airport Gate Scheduling** problem in the transportation industry is as follows: given a list of airplane arrival times and passenger connections, assign gates to planes so as to minimize the total distance passengers must walk to connecting gates.
- **Machine Learning (ML)** is a core problem of Artificial Intelligence. Most ML techniques require access to good-quality optimization heuristics as part of an inner loop computation that may be performed hundreds or thousands of times. The heuristic finds input/output pairs that constitute diverse samples of the near-optimal solution space of a given optimization problem.

The complexity class NP-OPT contains optimization problems (including (A1)) that are defined in terms of an objective function with a numerical result, as opposed to decision problems with binary results (e.g., Yes/No or True/False), which inhabit the more famous class NP.

Every problem  $P$  in NP can be reformulated (also called translated) as a problem  $P - OPT$  in NP-OPT. For example, the binary Satisfiability (SAT) problem, *Given Boolean expression  $B$ , does there exist an assignment of variables such that  $B$  evaluates to True?* can be translated to an equivalent problem in NP-OPT: *Given  $B - OPT$ , find an assignment of variables that maximizes the number of satisfied clauses*. The transformation guarantees that an optimal solution to SAT-OPT is a yes-answer to SAT. In this case, the maximum number of satisfied clauses equals the total number of clauses in  $B - OPT$ , then the answer to the binary problem is yes.

The translated SAT-OPT problem is called NP-HARD, because a polynomial time algorithm for SAT-OPT could be used to solve SAT, and by extension, every problem in NP could be solved in polynomial time. Problems that are both NP-HARD and in NP (i.e., binary decision problems) are called NP-COMPLETE. The famously open question *Does  $P = NP$ ?* captures the current unhappy state of knowledge about these problems: no polynomial time algorithm is known to exist, and no one can prove that they cannot exist.

**Solving Problems by Translation** Among many approaches to solving problems in NP and NP-OPT, solution-by-transformation has been studied for a handful of problems and algorithms.

This approach is attractive to practitioners when a single solver for target problem  $T$  can be applied to a wide variety of problems arising in practice: that is, when the overhead cost of translating individual inputs to match the formulation for  $T$  is less than the overhead cost of implementing a problem-specific solver for each new problem that arises.

The most widely studied versions of this approach involve a subset of problems formulated as (A1), known as integer linear problems, which can be solved in polynomial time when the objective function  $f(x)$  and constraints  $c_i(x)$  are all linear. Another common approach is to translate problems to SAT or SAT-OPT, for which sometimes-efficient heuristics are known.

The quadratic unconstrained binary optimization (QUBO) problem has also been considered as a general-purpose target formulation, especially for problems defined on graphs, before quantum computing arrived on the scene [100, 101]. The emergence of quantum annealing processors that solve QUBOs natively in hardware has sparked recent interest in QUBO and its variation, the Ising Model (IM) problem, often used in physics applications. The two problems are identical except for the change of a domain from binary variables  $x \in \{0, 1\}$  (QUBO) to spin variables  $s \in \{-1, +1\}$  (IM).

The theory of NP-completeness tells us that, in principle, any input for a problem formulated as (A1) can be transformed in polynomial time into a formulation that can be solved directly using a quantum computer. See [75, 76] for tutorials on formulating general optimization problems expressed by (A1) as QUBOs and IMs. However, the set of problems that can

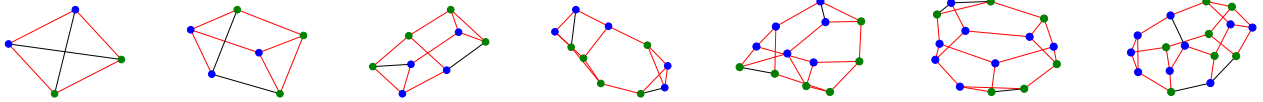


FIG. 28: **Graph Instances Chosen for the Benchmark Implementations.** For each problem size ranging from 4 to 16 in increments of 2, we used both QAOA and QA to solve the MaxCut problem for one 3-regular graph with that number of nodes. (For QA, larger graphs up to 320 nodes were also generated). In these graphs, one solution to the MaxCut problem is shown using colored nodes and edges. Nodes with different colors belong to the two sets of the solution cut. The number of red edges connecting nodes from different sets is the MaxCut for that graph.

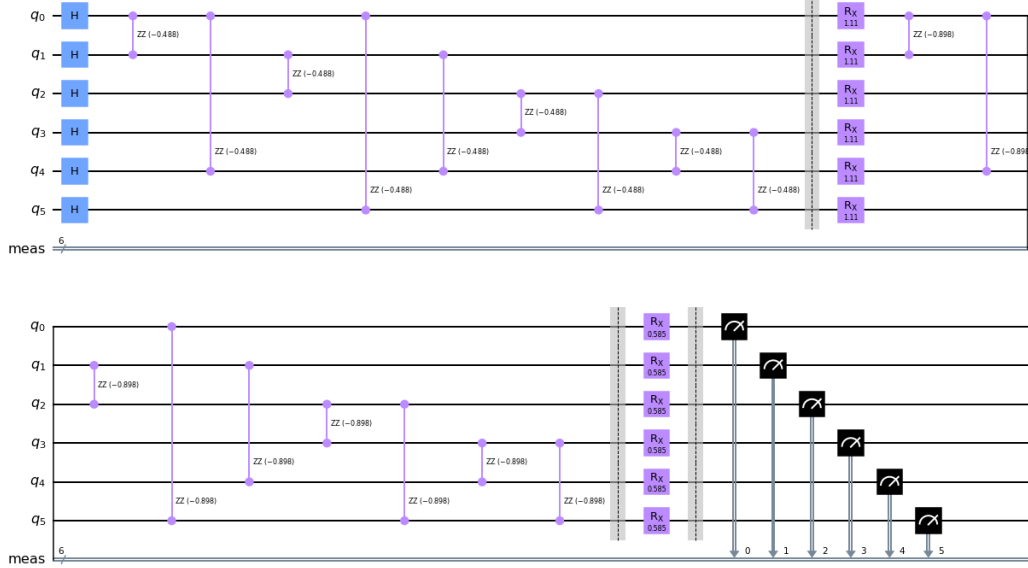


FIG. 29: **Sample QAOA Ansatz Circuit Diagram.** The quantum circuit shown here is the ansatz created for the MaxCut problem with 6 variables shown above, implemented using 2 rounds on 6 qubits. Each of the two sets of 9 parameterized RZZ gates maps to the circuit the edges contained within the graph and represents the problem Hamiltonian. The two sets of parameterized RX gates represent the mixer Hamiltonian. This circuit is an implementation of what is shown in Figure 4 for the specific graph used in the benchmark.

actually be tested on current quantum platforms is significantly restricted due to their small size.

#### Appendix B: Problem and Implementation Details

To generate the results presented in this paper, we executed the MaxCut benchmark on a single problem instance at each problem size (or number of qubits). The instance is a randomly chosen 3-regular graph at each size. A data set defining each instance is contained in the QED-C benchmark repository at <https://github.com/SRI-International/QC-App-Oriented-Benchmarks>. The benchmark can be modified to use other graphs if desired.

For reference, we present in Figure 28 some of the graphs that are used at different problem sizes. In each of these graphs, one solution to the MaxCut problem is shown using colored nodes and edges, as described in the caption.

In Figure 29 we show the QAOA ansatz circuit that is generated for the problem of size 6 (number of variables/qubits) that is used in this benchmark. The caption describes how

the components of the circuit represent the Hamiltonian that defines the problem.

Below, we show the  $J$  matrix required to specify the 6-variable Max-Cut problem for the quantum annealing hardware according to Equation 7.

$$J = \begin{bmatrix} 0 & -1 & 0 & 0 & -1 & -1 \\ -1 & 0 & -1 & 0 & -1 & 0 \\ 0 & -1 & 0 & -1 & 0 & -1 \\ 0 & 0 & -1 & 0 & -1 & -1 \\ -1 & -1 & 0 & -1 & 0 & 0 \\ -1 & 0 & -1 & -1 & 0 & 0 \end{bmatrix} \quad (B1)$$

[1] Ehsan Zahedinejad and Arman Zaribafian. Combinatorial optimization on gate model quantum computers: A survey, 2017. URL <https://arxiv.org/abs/1708.05294>.

[2] Daniel J. Egger, Claudio Gambella, Jakub Marecek, Scott McFaddin, Martin Mevissen, Rudy Raymond, Andrea Simonetto, Stefan Woerner, and Elena Yndurain. Quantum computing for finance: State-of-the-art and future prospects. *IEEE Transactions on Quantum Engineering*, 1:1–24, 2020. doi: 10.1109/TQE.2020.3030314.

[3] Catherine C. McGeoch and Cong Wang. Experimental evaluation of an adiabatic quantum system for combinatorial optimization. In *Proceedings of the ACM International Conference on Computing Frontiers*, CF ’13, New York, NY, USA, 2013. Association for Computing Machinery. ISBN 9781450320535. doi:10.1145/2482767.2482797. URL <https://doi.org/10.1145/2482767.2482797>.

[4] A.B. Finnila, M.A. Gomez, C. Sebenik, C. Stenson, and J.D. Doll. Quantum annealing: A new method for minimizing multi-dimensional functions. *Chemical Physics Letters*, 219(5):343 – 348, 1994. ISSN 0009-2614. doi:[https://doi.org/10.1016/0009-2614\(94\)00117-0](https://doi.org/10.1016/0009-2614(94)00117-0). URL <http://www.sciencedirect.com/science/article/pii/0009261494001170>.

[5] Tadashi Kadowaki and Hidetoshi Nishimori. Quantum annealing in the transverse Ising model. *Phys. Rev. E*, 58:5355–5363, Nov 1998. doi:10.1103/PhysRevE.58.5355.

[6] Edward Farhi, Jeffrey Goldstone, and Sam Gutmann. A quantum approximate optimization algorithm, 2014.

[7] Gavin E. Crooks. Performance of the Quantum Approximate Optimization Algorithm on the Maximum Cut Problem, November 2018.

[8] Jonathan Wurtz and Peter Love. MaxCut quantum approximate optimization algorithm performance guarantees for  $\text{Sp} > 1$ . *Physical Review A*, 103(4):042612, April 2021. doi: 10.1103/PhysRevA.103.042612.

[9] Immanuel Trummer and Christoph Koch. Multiple query optimization on the d-wave 2x adiabatic quantum computer, 2015. URL <https://arxiv.org/abs/1510.06437>.

[10] Yuchen Pang, Carleton Coffrin, Andrey Y. Lokhov, and Marc Vuffray. The potential of quantum annealing for rapid solution structure identification. *Constraints*, 26(1):1–25, Oct 2021. ISSN 1572-9354. doi:10.1007/s10601-020-09315-0. URL <https://doi.org/10.1007/s10601-020-09315-0>.

[11] Byron Tasseff, Tameem Albash, Zachary Morrell, Marc Vuffray, Andrey Y. Lokhov, Sidhant Misra, and Carleton Coffrin. On the emerging potential of quantum annealing hardware for combinatorial optimization, 2022. URL <https://arxiv.org/abs/2210.04291>.

[12] M. R. Garey, D. S. Johnson, and L. Stockmeyer. Some simplified NP-complete graph problems. *Theoretical Computer Science*, 1(3):237–267, February 1976. ISSN 0304-3975. doi: 10.1016/0304-3975(76)90059-1.

[13] Christos H. Papadimitriou and Mihalis Yannakakis. Optimization, approximation, and complexity classes. *Journal of Computer and System Sciences*, 43(3):425–440, 1991. ISSN 0022-0000. doi:[https://doi.org/10.1016/0022-0000\(91\)90023-X](https://doi.org/10.1016/0022-0000(91)90023-X). URL <https://www.sciencedirect.com/science/article/pii/002200009190023X>.

[14] Francisco Barahona, Martin Grötschel, Michael Jünger, and Gerhard Reinelt. An Application of Combinatorial Optimization to Statistical Physics and Circuit Layout Design. *Operations Research*, 36(3):493–513, June 1988. ISSN 0030-364X. doi:10.1287/opre.36.3.493.

[15] Bahram Alidaee, Gary A. Kochenberger, and Ahmad Ahmadian. 0-1 Quadratic programming approach for optimum solutions of two scheduling problems. *International Journal of Systems Science*, 25(2):401–408, February 1994. ISSN 0020-7721. doi:10.1080/00207729408928968.

[16] Application-Oriented Performance Benchmarks for Quantum Computing, 2015. URL <https://github.com/SRI-International/QC-App-Oriented-Benchmarks>.

[17] Thomas Lubinski, Sonika Johri, Paul Varosy, Jeremiah Coleman, Luning Zhao, Jason Necaise, Charles H. Baldwin, Karl Mayer, and Timothy Proctor. Application-Oriented Performance Benchmarks for Quantum Computing. (arXiv:2110.03137), December 2021.

[18] E. Knill, D. Leibfried, R. Reichle, J. Britton, R. B. Blakestad, J. D. Jost, C. Langer, R. Ozeri, S. Seidelin, and D. J. Wineland. Randomized benchmarking of quantum gates. *Phys. Rev. A*, 77: 012307, Jan 2008. doi:10.1103/PhysRevA.77.012307. URL <https://link.aps.org/doi/10.1103/PhysRevA.77.012307>.

[19] Easwar Magesan, J. M. Gambetta, and Joseph Emerson. Scalable and robust randomized benchmarking of quantum processes. *Phys. Rev. Lett.*, 106:180504, May 2011. doi: 10.1103/PhysRevLett.106.180504. URL <https://link.aps.org/doi/10.1103/PhysRevLett.106.180504>.

[20] Robin Blume-Kohout, John King Gamble, Erik Nielsen, Kenneth Rudinger, Jonathan Mizrahi, Kevin Fortier, and Peter Maunz. Demonstration of qubit operations below a rigorous fault tolerance threshold with gate set tomography. *Nat. Commun.*, 8:14485, February 2017. doi:10.1038/ncomms14485. URL <https://www.nature.com/articles/ncomms14485>.

[21] Sergio Boixo, Sergei V. Isakov, Vadim N. Smelyanskiy, Ryan Babbush, Nan Ding, Zhang Jiang, Michael J. Bremner, John M. Martinis, and Hartmut Neven. Characterizing quantum supremacy in near-term devices. *Nature Physics*, 14(6): 595–600, Apr 2018. ISSN 1745-2481. doi:10.1038/s41567-018-0124-x. URL <http://dx.doi.org/10.1038/s41567-018-0124-x>.

[22] Andrew W. Cross, Lev S. Bishop, Sarah Sheldon, Paul D. Nation, and Jay M. Gambetta. Validating quantum computers using randomized model circuits. *Physical Review A*, 100(3), Sep 2019. ISSN 2469-9934. doi:10.1103/physreva.100.032328. URL <http://dx.doi.org/10.1103/PhysRevA.100.032328>.

[23] Timothy Proctor, Kenneth Rudinger, Kevin Young, Erik Nielsen, and Robin Blume-Kohout. Measuring the capabilities of quantum computers, 2020.

[24] Andrew Wack, Hanhee Paik, Ali Javadi-Abhari, Petar Jurcevic, Ismael Faro, Jay M. Gambetta, and Blake R. Johnson. Quality, speed, and scale: three key attributes to measure the performance of near-term quantum computers, 2021. URL <https://arxiv.org/abs/2110.14108>.

[25] The Qiskit Team. Measuring quantum volume, Aug 2021. URL <https://qiskit.org/textbook/ch-quantum-hardware/measuring-quantum-volume.html>.

[26] Charles H. Baldwin, Karl Mayer, Natalie C. Brown, Ciarán Ryan-Anderson, and David Hayes. Re-examining the quantum volume test: Ideal distributions, compiler optimizations, confidence intervals, and scalable resource estimations. *Quantum*, 6:707, May 2022. ISSN 2521-327X. doi:10.22331/q-2022-05

09-707. URL <https://doi.org/10.22331/q-2022-05-09-707>.

[27] Daniel C Murphy and Kenneth R Brown. Controlling error orientation to improve quantum algorithm success rates. *Phys. Rev. A*, 99(3):032318, 2019. URL <https://journals.aps.org/pra/abstract/10.1103/PhysRevA.99.032318>.

[28] Elijah Pelofske, Andreas Bartschi, and Stephan Eidenbenz. Quantum volume in practice: What users can expect from NISQ devices. *IEEE Transactions on Quantum Engineering*, 3:1–19, 2022. doi:10.1109/tqe.2022.3184764. URL <https://doi.org/10.1109%2Ftqe.2022.3184764>.

[29] Scott Aaronson. Turn down the quantum volume, Mar 2020. URL <https://www.scottaaronson.com/blog/?p=4649>.

[30] Robin Blume-Kohout and Kevin C. Young. A volumetric framework for quantum computer benchmarks. *Quantum*, 4: 362, November 2020. ISSN 2521-327X. doi:10.22331/q-2020-11-15-362. URL <https://doi.org/10.22331/q-2020-11-15-362>.

[31] Timothy Proctor, Stefan Seritan, Erik Nielsen, Kenneth Rudinger, Kevin Young, Robin Blume-Kohout, and Mohan Sarovar. Establishing trust in quantum computations, 2022. URL <https://arxiv.org/abs/2204.07568>.

[32] Ang Li, Samuel Stein, Sriram Krishnamoorthy, and James Ang. Qasmbench: A low-level qasm benchmark suite for nisq evaluation and simulation, 2020. URL <https://arxiv.org/abs/2005.13018>.

[33] Teague Tomesh, Pranav Gokhale, Victory Omole, Gokul Subramanian Ravi, Kaitlin N. Smith, Joshua Viszlai, Xin-Chuan Wu, Nikos Hardavellas, Margaret R. Martonosi, and Frederic T. Chong. Supermarq: A scalable quantum benchmark suite, 2022. URL <https://arxiv.org/abs/2202.11045>.

[34] Huub Donkers, Koen Mesman, Zaid Al-Ars, and Matthias Möller. Qpack scores: Quantitative performance metrics for application-oriented quantum computer benchmarking, 2022. URL <https://arxiv.org/abs/2205.12142>.

[35] Algorithmic Qubits: A Better Single-Number Metric. <https://ionq.com/posts/february-23-2022-algorithmic-qubits>, 2022. IonQ Post.

[36] Ernst Hellinger. Neue begründung der theorie quadratischer formen von unendlichvielen veränderlichen. *Journal für die reine und angewandte Mathematik*, 1909(136):210–271, 1909.

[37] Blake Johnson and Ismael Faro. Ibm quantum delivers 120x speedup of quantum workloads with qiskit runtime, May 2021. URL <https://research.ibm.com/blog/120x-quantum-speedup?lnk=ushpv18re2>.

[38] K. Bertels, A. Sarkar, T. Hubregtsen., M. Serrao, A. A. Mouedenne, A. Yadav, A. Krol, and I. Ashraf. Quantum computer architecture: Towards full-stack quantum accelerators. *2020 Design, Automation & Test in Europe Conference & Exhibition (DATE)*, Mar 2020. doi:10.23919/date48585.2020.9116502. URL <http://dx.doi.org/10.23919/DATE48585.2020.9116502>.

[39] Matthias Möller and Cornelis Vuik. On the impact of quantum computing technology on future developments in high-performance scientific computing. *Ethics and Information Technology*, 19(4):253–269, Aug 2017. ISSN 1572-8439. doi:10.1007/s10676-017-9438-0. URL <http://dx.doi.org/10.1007/s10676-017-9438-0>.

[40] Yudong Cao and Timothy Hirzel. Quantum acceleration in 2020, Dec 2020. URL <https://www.infoq.com/articles/quantum-acceleration-2020/>.

[41] Frank Arute, Kunal Arya, Ryan Babbush, Dave Bacon, Joseph C Bardin, Rami Barends, Rupak Biswas, Sergio Boixo, Fernando G S L Brandao, David A Buell, Brian Burkett, Yu Chen, Zijun Chen, Ben Chiaro, Roberto Collins, William Courtney, Andrew Dunsworth, Edward Farhi, Brooks Foxen, Austin Fowler, Craig Gidney, Marissa Giustina, Rob Graff, Keith Guerin, Steve Habegger, Matthew P Harrigan, Michael J Hartmann, Alan Ho, Markus Hoffmann, Trent Huang, Travis S Humble, Sergei V Isakov, Evan Jeffrey, Zhang Jiang, Dvir Kafri, Kostyantyn Kechedzhi, Julian Kelly, Paul V Klimov, Sergey Knysh, Alexander Korotkov, Fedor Kostritsa, David Landhuis, Mike Lindmark, Erik Lucero, Dmitry Lyakh, Salvatore Mandrà, Jarrod R McClean, Matthew McEwen, Anthony Megrant, Xiao Mi, Kristel Michelsen, Masoud Mohseni, Josh Mutus, Ofer Naaman, Matthew Neeley, Charles Neill, Murphy Yuezen Niu, Eric Ostby, Andre Petukhov, John C Platt, Chris Quintana, Eleanor G Rieffel, Pedram Roushan, Nicholas C Rubin, Daniel Sank, Kevin J Satzinger, Vadim Smelyanskiy, Kevin J Sung, Matthew D Trevithick, Amit Vainsencher, Benjamin Villalonga, Theodore White, Z Jamie Yao, Ping Yeh, Adam Zalcman, Hartmut Neven, and John M Martinis. Quantum supremacy using a programmable superconducting processor. *Nature*, 574(7779):505–510, 2019. ISSN 0028-0836, 1476-4687. doi:10.1038/s41586-019-1666-5. URL <http://dx.doi.org/10.1038/s41586-019-1666-5>.

[42] Han-Sen Zhong, Hui Wang, Yu-Hao Deng, Ming-Cheng Chen, Li-Chao Peng, Yi-Han Luo, Jian Qin, Dian Wu, Xing Ding, Yi Hu, Peng Hu, Xiao-Yan Yang, Wei-Jun Zhang, Hao Li, Yuxuan Li, Xiao Jiang, Lin Gan, Guangwen Yang, Lixing You, Zhen Wang, Li Li, Nai-Le Liu, Chao-Yang Lu, and Jian-Wei Pan. Quantum computational advantage using photons. *Science*, 370(6523):1460–1463, 2020. ISSN 0036-8075, 1095-9203. doi:10.1126/science.abe8770. URL <http://dx.doi.org/10.1126/science.abe8770>.

[43] Hristo N. Djidjev, Guillaume Chapuis, Georg Hahn, and Guillaume Rizk. Efficient combinatorial optimization using quantum annealing, 2018. URL <https://arxiv.org/abs/1801.08653>.

[44] Byron Tasseff, Tameem Albash, Zachary Morrell, Marc Vuffray, Andrey Y. Lokhov, Sidhant Misra, and Carleton Coffrin. On the emerging potential of quantum annealing hardware for combinatorial optimization, 2022. URL <https://arxiv.org/abs/2210.04291>.

[45] Mark Johnson, Mohammad Amin, S Gildert, Trevor Lanting, F Hamze, N Dickson, R Harris, Andrew Berkley, Jan Johansson, Paul Bunyk, E Chapple, C Enderud, Jeremy Hilton, Kamran Karimi, E Ladizinsky, Nicolas Ladizinsky, T Oh, I Perminov, C Rich, and Geordie Rose. Quantum annealing with manufactured spins. *Nature*, 473:194–8, 05 2011. doi:10.1038/nature10012.

[46] Alejandro Perdomo-Ortiz, Alexander Feldman, Asier Ozeta, Sergei V. Isakov, Zheng Zhu, Bryan O’Gorman, Helmut G. Katzgraber, Alexander Diedrich, Hartmut Neven, Johan de Kleer, Brad Lackey, and Rupak Biswas. Readiness of quantum optimization machines for industrial applications. *Physical Review Applied*, 12(1), jul 2019. doi:10.1103/physrevapplied.12.014004. URL <https://doi.org/10.1103%2Fphysrevapplied.12.014004>.

[47] Bikas K Chakrabarti and Sudip Mukherjee. Quantum annealing and computation, 2022. URL <https://arxiv.org/abs/2203.15839>.

[48] Neil G. Dickson, M. William Johnson, Mohammad H. S. Amin, R. Harris, F. Altomare, Andrew J. Berkley, Paul I. Bunyk, J. Cai, E. M. Chapple, P. Chavez, Florentin Cioată, T. Cirip, P. Debuen, Marshall Drew-Brook, C. Enderud, S. Gildert, Firas Hamze, Jeremy P. Hilton, E. Hoskinson, Kamran Karimi, Eric Ladizinsky, Nicolas Ladizinsky, Trevor Lanting, Timothy Ma-

hon, Richard Bryon Neufeld, Travis Oh, I. G. Perminov, C P Petroff, Anthony J. Przybysz, Chris Rich, P. Spear, Adi Tcaciu, Murray C. Thom, Elena Tolkacheva, Sergey Uchaikin, J. Wang, A. B. Wilson, Zeeya Merali, and Geordie Rose. Thermally assisted quantum annealing of a 16-qubit problem. *Nature communications*, 4:1903, 2013.

[49] T. Lanting, A. J. Przybysz, A. Yu. Smirnov, F. M. Spedalieri, M. H. Amin, A. J. Berkley, R. Harris, F. Altomare, S. Boixo, P. Bunyk, N. Dickson, C. Enderud, J. P. Hilton, E. Hoskinson, M. W. Johnson, E. Ladizinsky, N. Ladizinsky, R. Neufeld, T. Oh, I. Perminov, C. Rich, M. C. Thom, E. Tolkacheva, S. Uchaikin, A. B. Wilson, and G. Rose. Entanglement in a quantum annealing processor. *Physical Review X*, 4(2), may 2014. doi:10.1103/physrevx.4.021041. URL <https://doi.org/10.1103/physrevx.4.021041>.

[50] Tristan Zaborniak and Rogério de Sousa. Benchmarking hamiltonian noise in the d-wave quantum annealer. *IEEE Transactions on Quantum Engineering*, 2:1–6, 2021. doi: 10.1109/TQE.2021.3050449.

[51] Jon Nelson, Marc Vuffray, Andrey Y. Lokhov, and Carleton Coffrin. Single-qubit fidelity assessment of quantum annealing hardware. *IEEE Transactions on Quantum Engineering*, 2: 1–10, 2021. doi:10.1109/TQE.2021.3092710.

[52] Marc Vuffray, Carleton Coffrin, Yaroslav A. Kharkov, and Andrey Y. Lokhov. Programmable quantum annealers as noisy gibbs samplers. *PRX Quantum*, 3:020317, Apr 2022. doi: 10.1103/PRXQuantum.3.020317. URL <https://link.aps.org/doi/10.1103/PRXQuantum.3.020317>.

[53] James King, Sheir Yarkoni, Mayssam M. Nevisi, Jeremy P. Hilton, and Catherine C. McGeoch. Benchmarking a quantum annealing processor with the time-to-target metric, 2015. URL <https://arxiv.org/abs/1508.05087>.

[54] David Subires, Fernando J. Gómez-Ruiz, Antonia Ruiz-García, Daniel Alonso, and Adolfo del Campo. Benchmarking quantum annealing dynamics: The spin-vector langevin model. *Physical Review Research*, 4(2), may 2022. doi: 10.1103/physrevresearch.4.023104. URL <https://doi.org/10.1103/physrevresearch.4.023104>.

[55] Antika Sinha. Development of research network on quantum annealing computation and information using google scholar data, 2022. URL <https://arxiv.org/abs/2206.02176>.

[56] S. Kirkpatrick, C. D. Gelatt, and M. P. Vecchi. Optimization by simulated annealing. *Science*, 220(4598):671–680, 1983. doi:10.1126/science.220.4598.671. URL <https://www.science.org/doi/abs/10.1126/science.220.4598.671>.

[57] Charlie J. Geyer. Parallel tempering. In E. M. Keramidas and S. M. Kaufman, editors, *Computing Science and Statistics Proceedings of the 23rd Symposium on the Interface*, page 156, New York, 1991. American Statistical Association.

[58] Bor1928Zheng Zhu, Andrew J. Ochoa, and Helmut G. Katzgraber. Efficient cluster algorithm for spin glasses in any space dimension. *Phys. Rev. Lett.*, 115:077201, August 2015. doi:<https://doi.org/10.1103/PhysRevLett.115.077201>. URL <https://link.aps.org/doi/10.1103/PhysRevLett.115.077201>.

[59] Carleton Coffrin, Harsha Nagarajan, and Russell Bent. Evaluating Ising processing units with integer programming. In Louis-Martin Rousseau and Kostas Stergiou, editors, *Integration of Constraint Programming, Artificial Intelligence, and Operations Research*, pages 163–181, Cham, 2019. Springer International Publishing. ISBN 978-3-030-19212-9.

[60] Itay Hen, Joshua Job, Tameem Albash, Troels F. Rønnow, Matthias Troyer, and Daniel A. Lidar. Probing for quantum speedup in spin-glass problems with planted solutions. *Phys. Rev. A*, 92:042325, Oct 2015. doi: 10.1103/PhysRevA.92.042325. URL <https://link.aps.org/doi/10.1103/PhysRevA.92.042325>.

[61] Dilina Perera, Inimfon Akpabio, Firas Hamze, Salvatore Mandrà, Nathan Rose, Maliheh Aramon, and Helmut G. Katzgraber. CHOOK – a comprehensive suite for generating binary optimization problems with planted solutions, 2020. URL <https://arxiv.org/abs/2005.14344>.

[62] Matthew Kowalsky, Tameem Albash, Itay Hen, and Daniel A. Lidar. 3-regular 3-xorsat planted solutions benchmark of classical and quantum heuristic optimizers. 2021. doi:10.1088/2058-9565/ac4d1b.

[63] Juneseo Lee, Alicia B. Magann, Herschel A. Rabitz, and Christian Arenz. Progress toward favorable landscapes in quantum combinatorial optimization. *Physical Review A*, 104(3), sep 2021. doi:10.1103/physreva.104.032401. URL <https://doi.org/10.1103%2Fphysreva.104.032401>.

[64] Jonathan Ward, Johannes Otterbach, Gavin Crooks, Nicholas Rubin, and Marcus da Silva. QAOA Performance Benchmarks using Max-Cut. In *APS March Meeting Abstracts*, volume 2018 of *APS Meeting Abstracts*, page R15.007, January 2018.

[65] Gavin E. Crooks. Performance of the quantum approximate optimization algorithm on the maximum cut problem, 2018. URL <https://arxiv.org/abs/1811.08419>.

[66] Leo Zhou, Sheng-Tao Wang, Soonwon Choi, Hannes Pichler, and Mikhail D. Lukin. Quantum approximate optimization algorithm: Performance, mechanism, and implementation on near-term devices. *Physical Review X*, 10(2), jun 2020. doi: 10.1103/physrevx.10.021067. URL <https://doi.org/10.1103%2Fphysrevx.10.021067>.

[67] Tameem Albash and Daniel A. Lidar. Demonstration of a scaling advantage for a quantum annealer over simulated annealing. *Physical Review X*, 8(3), jul 2018. doi: 10.1103/physrevx.8.031016. URL <https://doi.org/10.1103%2Fphysrevx.8.031016>.

[68] S. Ebadi, A. Keesling, M. Cain, T. T. Wang, H. Levine, D. Bluvstein, G. Semeghini, A. Omran, J.-G. Liu, R. Samajdar, X.-Z. Luo, B. Nash, X. Gao, B. Barak, E. Farhi, S. Sachdev, N. Gemelke, L. Zhou, S. Choi, H. Pichler, S.-T. Wang, M. Greiner, V. Vuletić, and M. D. Lukin. Quantum optimization of maximum independent set using rydberg atom arrays. *Science*, 376(6598):1209–1215, 2022. doi: 10.1126/science.abe6587. URL <https://www.science.org/doi/abs/10.1126/science.abe6587>.

[69] Troels F. Rønnow, Zhihui Wang, Joshua Job, Sergio Boixo, Sergei V. Isakov, David Wecker, John M. Martinis, Daniel A. Lidar, and Matthias Troyer. Defining and detecting quantum speedup. *Science*, 345(6195):420–424, jul 2014. doi: 10.1126/science.1252319. URL <https://doi.org/10.1126/science.1252319>.

[70] Salvatore Mandrà and Helmut G. Katzgraber. A deceptive step towards quantum speedup detection. *Quantum Science and Technology*, 3(4):04LT01, jul 2018. doi:10.1088/2058-9565/aac8b2. URL <https://doi.org/10.1088%2F2058-9565%2Faac8b2>.

[71] Jernej Rudi Finžgar, Philipp Ross, Leonhard Hölscher, Johannes Klepsch, and Andre Luckow. Quark: A framework for quantum computing application benchmarking, 2022. URL <https://arxiv.org/abs/2202.03028>.

[72] Ward van der Schoot, Daan Leermakers, Robert Wezeman, Niels Neumann, and Frank Phillipson. Evaluating the q-score of quantum annealers. In *2022 IEEE International Conference on Quantum Software (QSW)*. IEEE, jul 2022. doi: 10.1109/qsw55613.2022.00017. URL <https://doi.org/10.1109/qsw55613.2022.00017>.

.1109%2Fqsw55613.2022.00017.

[73] Daniel Beaulieu and Anh Pham. Evaluating performance of hybrid quantum optimization algorithms for maxcut clustering using ibm runtime environment, 2021. URL <https://arxiv.org/abs/2112.03199>.

[74] Johan Håstad. Some optimal inapproximability results. *Journal of the ACM*, 48(4):798–859, July 2001. ISSN 0004-5411. doi: 10.1145/502090.502098.

[75] Fred Glover, Gary Kochenberger, and Yu Du. A tutorial on formulating and using qubo models, 2018. URL <https://arxiv.org/abs/1811.11538>.

[76] Andrew Lucas. Ising formulations of many NP problems. *Frontiers in Physics*, 2, 2014. doi:10.3389/fphy.2014.00005. URL <https://doi.org/10.3389%2Ffphy.2014.00005>.

[77] Edward Farhi, Jeffrey Goldstone, and Sam Gutmann. A Quantum Approximate Optimization Algorithm. (arXiv:1411.4028), November 2014. doi:10.48550/arXiv.1411.4028.

[78] M. Cerezo, Andrew Arrasmith, Ryan Babbush, Simon C. Benjamin, Suguru Endo, Keisuke Fujii, Jarrod R. McClean, Kosuke Mitarai, Xiao Yuan, Lukasz Cincio, and Patrick J. Coles. Variational quantum algorithms. *Nature Reviews Physics*, 3(9): 625–644, aug 2021. doi:10.1038/s42254-021-00348-9. URL <https://doi.org/10.1038%2Fs42254-021-00348-9>.

[79] M. Born and V. Fock. Beweis des adiabatensatzes. *Zeitschrift für Physik*, 51(3):165–180, 1928. doi:10.1007/BF01343193. URL <https://doi.org/10.1007/BF01343193>.

[80] Tosio Kato. On the adiabatic theorem of quantum mechanics. *Journal of the Physical Society of Japan*, 5(6):435–439, 1950. doi:10.1143/JPSJ.5.435. URL <https://doi.org/10.1143/JPSJ.5.435>.

[81] Sabine Jansen, Mary-Beth Ruskai, and Ruedi Seiler. Bounds for the adiabatic approximation with applications to quantum computation. *Journal of Mathematical Physics*, 48(10):102111, 2007. doi:10.1063/1.2798382. URL <https://doi.org/10.1063/1.2798382>.

[82] Vicky Choi. Minor-embedding in adiabatic quantum computation: I. the parameter setting problem. *Quantum Information Processing*, 7:193–209, 2008.

[83] Lennart Bittel and Martin Kliesch. Training Variational Quantum Algorithms Is NP-Hard. *Physical Review Letters*, 127(12):120502, September 2021. doi: 10.1103/PhysRevLett.127.120502.

[84] Madita Willsch, Dennis Willsch, Fengping Jin, Hans De Raedt, and Kristel Michielsen. Benchmarking the quantum approximate optimization algorithm. *Quantum Information Processing*, 19(7), jun 2020. doi:10.1007/s11128-020-02692-8. URL <https://doi.org/10.1007%2Fs11128-020-02692-8>.

[85] Jason Larkin, Matías Jonsson, Daniel Justice, and Gian Giacomo Guerreschi. Evaluation of QAOA based on the approximation ratio of individual samples, December 2020.

[86] Phillip C. Lotshaw, Travis S. Humble, Rebekah Herrman, James Ostrowski, and George Siopsis. Empirical performance bounds for quantum approximate optimization. *Quantum Information Processing*, 20(12), nov 2021. doi:10.1007/s11128-021-03342-3. URL <https://doi.org/10.1007%2Fs11128-021-03342-3>.

[87] Qiskit Runtime. <https://quantum-computing.ibm.com/lab/docs/iql/runtime/>, 2021. IBM Quantum Lab.

[88] Introducing Amazon Braket Hybrid Jobs. <https://aws.amazon.com/blogs/aws/introducing-amazon-braket-hybrid-jobs-set-up-monitor-and-efficiently-run-hybrid-quantum-classical-workloads/>, 2021. Amazon Braket.

[89] Michael JD Powell. A view of algorithms for optimization without derivatives. *Mathematics Today-Bulletin of the Institute of Mathematics and its Applications*, 43(5):170–174, 2007.

[90] Panagiotis KI Barkoutsos, Giacomo Nannicini, Anton Robert, Ivano Tavernelli, and Stefan Woerner. Improving Variational Quantum Optimization using CVaR. *Quantum*, 4:256, April 2020. doi:10.22331/q-2020-04-20-256.

[91] Li Li, Minjie Fan, Marc Coram, Patrick Riley, and Stefan Leichenauer. Quantum optimization with a novel Gibbs objective function and ansatz architecture search. *Physical Review Research*, 2(2):023074, April 2020. doi: 10.1103/PhysRevResearch.2.023074.

[92] Jarrod R. McClean, Sergio Boixo, Vadim N. Smelyanskiy, Ryan Babbush, and Hartmut Neven. Barren plateaus in quantum neural network training landscapes. *Nature Communications*, 9(1):4812, November 2018. ISSN 2041-1723. doi: 10.1038/s41467-018-07090-4.

[93] M. Cerezo, Akira Sone, Tyler Volkoff, Lukasz Cincio, and Patrick J. Coles. Cost function dependent barren plateaus in shallow parametrized quantum circuits. *Nature Communications*, 12(1):1791, March 2021. ISSN 2041-1723. doi: 10.1038/s41467-021-21728-w.

[94] Samson Wang, Enrico Fontana, M. Cerezo, Kunal Sharma, Akira Sone, Lukasz Cincio, and Patrick J. Coles. Noise-induced barren plateaus in variational quantum algorithms. *Nature Communications*, 12(1):6961, November 2021. ISSN 2041-1723. doi:10.1038/s41467-021-27045-6.

[95] Carlos Ortiz Marrero, Mária Kieferová, and Nathan Wiebe. Entanglement Induced Barren Plateaus. (arXiv:2010.15968), March 2021. doi:10.48550/arXiv.2010.15968.

[96] Jonathan Wurtz and Danylo Lykov. Fixed-angle conjectures for the quantum approximate optimization algorithm on regular MaxCut graphs. *Physical Review A*, 104(5):052419, November 2021. doi:10.1103/PhysRevA.104.052419.

[97] V. Akshay, D. Rabinovich, E. Campos, and J. Biamonte. Parameter concentrations in quantum approximate optimization. *Physical Review A*, 104(1):L010401, July 2021. ISSN 2469-9926, 2469-9934. doi:10.1103/PhysRevA.104.L010401.

[98] David Bernal Neira, Davide Venturelli, Filip Wudarski, and Eleanor Rieffel. Benchmarking the operation of quantum heuristics and ising machines: Scoring parameter setting strategies on real world optimization applications. In *APS March Meeting Abstracts*, volume 2022, pages F38–005, 2022.

[99] Stochastic benchmark. <https://github.com/usra-riac/s/stochastic-benchmark>, 2022.

[100] Endre Boros, Peter L Hammer, and Gabriel Tavares. Local search heuristics for quadratic unconstrained binary optimization (qubo). *Journal of Heuristics*, 13(2):99–132, 2007.

[101] Gary Kochenberger, Jin-Kao Hao, Fred Glover, Mark Lewis, Zhipeng Lü, Haibo Wang, and Yang Wang. The unconstrained binary quadratic programming problem: a survey. *Journal of combinatorial optimization*, 28(1):58–81, 2014.